ORIGINAL

Faulting, mass-wasting and deposition in an active dextral shear zone, the Gulf of Saros and the NE Aegean Sea, NW Turkey

Timur Ustaömer · Erkan Gökaşan · Hüseyin Tur ·
Tolga Görüm · Fatma Gül Batuk · Doğan Kalafat ·
Hakan Alp · Berkan Ecevitoğlu · Halim Birkan

Abstract Structural, mass-wasting and sedimentation processes along an active dextral shear zone beneath the Gulf of Saros and the NE Aegean Sea were investigated on the basis of new high-resolution swath bathymetric data and multi-channel seismics. A long history of dextral shearing operating since the Pliocene culminated in the formation of a NE-SW-trending, ca. 800-m-deep basin (the so-called inner basin) in this region, which is bordered by a broad shelf along its northern and eastern sides and a narrow shelf at the southern side. The western extension of the North Anatolian Fault Zone (the Ganos Fault) cuts the eastern shelf along a narrow deformation zone, and ends sharply at the toe of the slope, where the strain is taken up by two NE-SW-oriented fault zones. These two fault zones cut the basin floor along its central axis and generate a new, Riedel-type pull-apart basin (the so-called inner depression). According to the bathymetric and seismic data, these basin boundary fault zones are very recent features. The northern boundary of the inner depression is a through-going fault comprising several NE-SW- and E-W-oriented, overlapping fault segments. The southern boundary fault zone, on the other hand, consists of spectacular en-echelon fault systems aligned in NE–SW and WNW–ESE directions. These en-echelon faults accommodate both dextral and vertical motions, thereby generating block rotations along their horizontal axis. As the basin margins retreat, the basin widens continuously by mass-wasting of the slopes of the inner basin. The mass-wasting, triggered by active tectonics, occurs by intense landsliding and channel erosion. The eroded material is transported into the deep basin, where it is deposited in a series of deep-sea fans and slumps. The high sedimentation rate is reflected in an over 1,500-m-thick basin fill which has accumulated in Pliocene–Quaternary times.

T. Ustaömer (✉)
Faculty of Engineering, Department of Geology,
Istanbul University, Avcılar, 34850 Istanbul, Turkey
e-mail: timur@istanbul.edu.tr

E. Gökaşan · T. Görüm
Natural Sciences Research Center, Yıldız Technical University,
Beşiktaş, 34349 Istanbul, Turkey

H. Tur · H. Alp
Faculty of Engineering, Department of Geophysics,
Istanbul University, Avcılar, 34850 Istanbul, Turkey

F. G. Batuk
Faculty of Civil Engineering,
Department of Geodesy and Fotogrametric Engineering,
Yıldız Technical University, Beşiktaş, 34349 Istanbul, Turkey

D. Kalafat
Kandilli Observatory and Earthquake Research Institute,
Boğaziçi University,
Çengelköy,
34684 Istanbul, Turkey

B. Ecevitoğlu
Faculty of Engineering,
Department of Geophysical Engineering,
Ankara University,
Tandoğan,
06100 Ankara, Turkey

H. Birkan
Department of Navigation, Hydrography and Oceanography,
Turkish Navy, Çubuklu,
81647 Istanbul, Turkey

Introduction

The NE-SW-oriented Gulf of Saros is a westward-widening and -deepening, triangular marine embayment in the northeastern Aegean Sea, with a water depth of >645 m (Fig. 1a). It constitutes the eastern extension of the North Aegean Trough (NAT), and is separated from the Marmara Sea by the Thrace Peninsula and its NE-SW-oriented narrow extension, the Gelibolu Peninsula (Fig. 1b). The Gulf of Saros was formed in the course of the postglacial transgression across the Quaternary Saros Basin fill and its basement units (Çağatay et al. 1998; Tüysüz et al. 1998). A NE-SW-trending dextral strike–slip fault, termed the Ganos Fault, dissects the Gelibolu Peninsula in the north and then enters the Gulf of Saros. Although its kinematic history may date back to the late Oligocene (Zattin et al. 2005), the onland section of the Ganos Fault shows low seismic activity and is regarded as the western continuation of the North Anatolian Fault Zone (NAFZ) in the Marmara Sea.

The NAFZ is a 1,200-km-long, dextral strike–slip fault, extending across northern Anatolia from the Karlıova region in the east to the northern Aegean Sea in the west (Ketin 1948, 1968; Şengör 1979; Şengör et al. 1985, 2005; Barka and Kadinsky-Cade 1988; Barka 1992; Şaroğlu et al. 1992; Barka and Reilinger 1997; Fig. 1a). Immediately east of the Marmara Sea, this fault zone splits into three segments (Fig. 1a), the most active of which is the northern segment which extends into the Marmara Sea via the Gulf of İzmit, thereby dissecting the approximately E-W-oriented, deep Marmara Basin. Detailed swath bathymetric and seismic data collected after the Kocaeli earthquake of 17th August 1999 revealed the presence of several fault segments within the Marmara Sea. An analysis of these faults and their cross-cutting relationship with the sedimentary fill indicates that a single dextral fault zone runs from the Gulf of İzmit through the Ganos Mountain system along the centre of the deep Marmara Trough (Fig. 1a; Gökaşan et al. 2001, 2002, 2003; İmren et al. 2001; Le Pichon et al. 2001; Gazioğlu et al. 2002; Kuşçu et al. 2002; Demirbağ et al. 2003; Rangin et al. 2004; Şengör et al. 2005). Geodetic velocities and the offsets of particular morphological features at the seabed suggest that the North

Fig. 1 a Digital elevation model showing the traces of the North and East Anatolian fault zones. Note that the North Anatolian Fault splits into three segments to the east of the Marmara Sea, the northern branch of which runs through the Marmara Sea and enters the Gulf of Saros and the North Aegean Trough. The box indicates the location of the study area. b Simplified geological map of the land surrounding the study area (compiled from Erol and Nuttal 1973; Sümengen et al. 1987; Siyako et al. 1989), superimposed on a digital elevation model. The solid lines indicate the locations of the available seismic profiles. The red lines show the seismic profiles used in this paper. GF Ganos Fault, GI Gulf of İzmit, GMS Ganos Mountains, GS Gulf of Saros, MS Marmara Sea, TP Thrace Peninsula
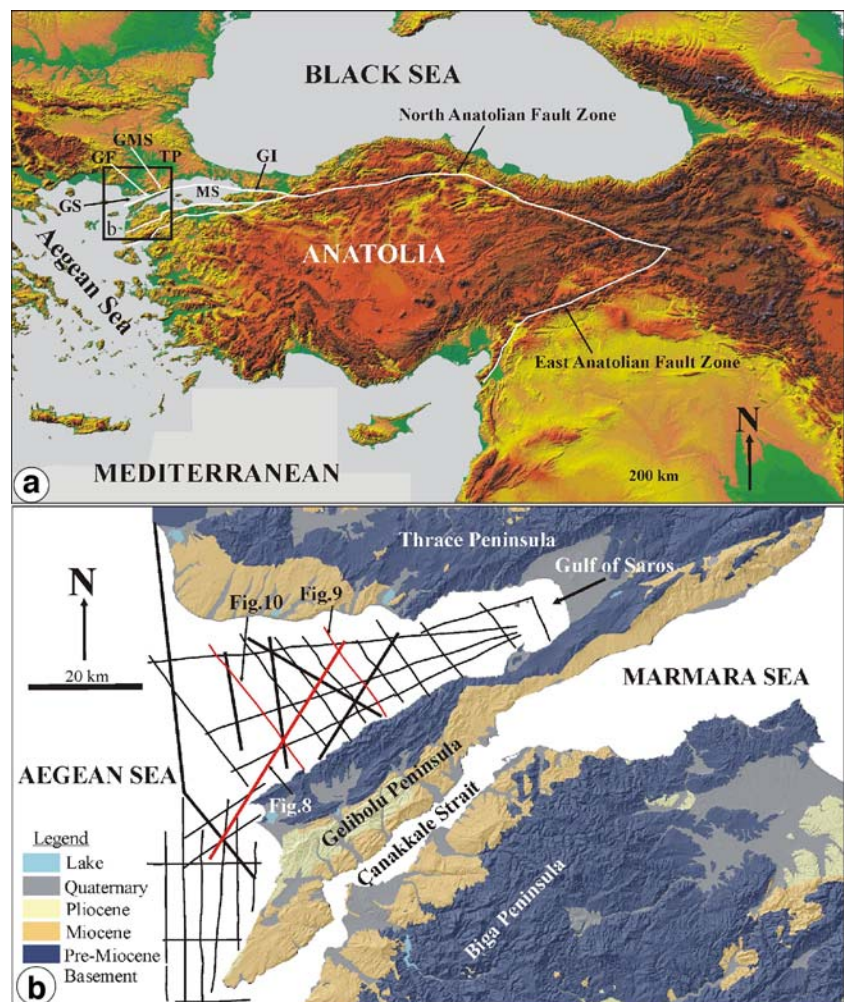
Anatolian Fault in the Marmara Sea is a young feature, dating back to 200 ka B.P. (Le Pichon et al. 2001).

This central fault changes its E–W orientation by 17° towards the west, and runs through the Gelibolu Peninsula as a NE-SW-trending fault. The Eocene to Oligocene units on the Ganos Mountains to the north of this fault are sharply separated from Miocene and younger sediments located in the south. The Ganos Mountains are considered to have uplifted as a restraining ridge formed due to the bend along this fault (Okay et al. 2004). The fault segment (the Ganos Fault) has been mapped during extensive field studies following a large earthquake (M_w 7.4) in 1912 (Gutzwiller 1923; Ambraseys and Finkel 1987; Barka and Kadinsky-Cade 1988; Tüysüz et al. 1998; Yaltırak et al. 1998, 2002; Armijo et al. 1999, 2002, 2005; Okay et al. 1999, 2004; Yaltırak and Alpar 2002; Altunel et al. 2004; Seeber et al. 2004). Notably, a 40- to 50-km surface rupture was inferred to have occurred under the Gulf of Saros (Karabulut et al. 2006).

The Gulf of Saros is located in a complex tectonic setting where the Miocene to Recent Aegean extensional province interacts with the western extension of the Quaternary North Anatolian Fault Zone. The age and the kinematics of the opening of the Saros Basin are still being hotly debated, suggested ages ranging from Oligocene (Saner 1985; Coşkun 2000) to Pliocene–Quaternary (Çağatay et al. 1998; Tüysüz et al. 1998; Yaltırak et al. 1998; Yaltırak and Alpar 2002). Three different mechanisms for the opening of the Saros Basin have been suggested. These range from pure extension- (a graben; Pfannenstiel 1944; Saner 1985, Fig. 2a), to strike–slip- (pull-apart basin: Barka and Kadinsky-Cade 1988; Tüysüz et al. 1998, Fig. 2b; or a trans-tensional basin: Görür et al. 1997; Çağatay et al. 1998, Fig. 2c; Saatçılar et al. 1999; Kurt et al. 2000, Fig. 2d; McNeill et al. 2004), or tectonic escape-related basin formation processes (Yaltırak et al. 1998; Yaltırak and Alpar 2002, Fig. 2e). According to the latter model, the south-westerly escape of a wedge-shaped middle block in response to NW-SE-oriented compression has formed the Saros Basin. The dextral Ganos Fault along the northern margin, and the sinistral Gelibolu Fault along the southern margin of the Saros Basin accommodated this tectonically escaped middle block.

Fig. 2 Existing models for the kinematics of the Ganos Fault and the evolution of the Saros Gulf (see text for explanation). a Saner (1985), b Tüysüz et al. (1998), c Çağatay et al. (1998), d Kurt et al. (2000), e Yaltırak and Alpar (2002)
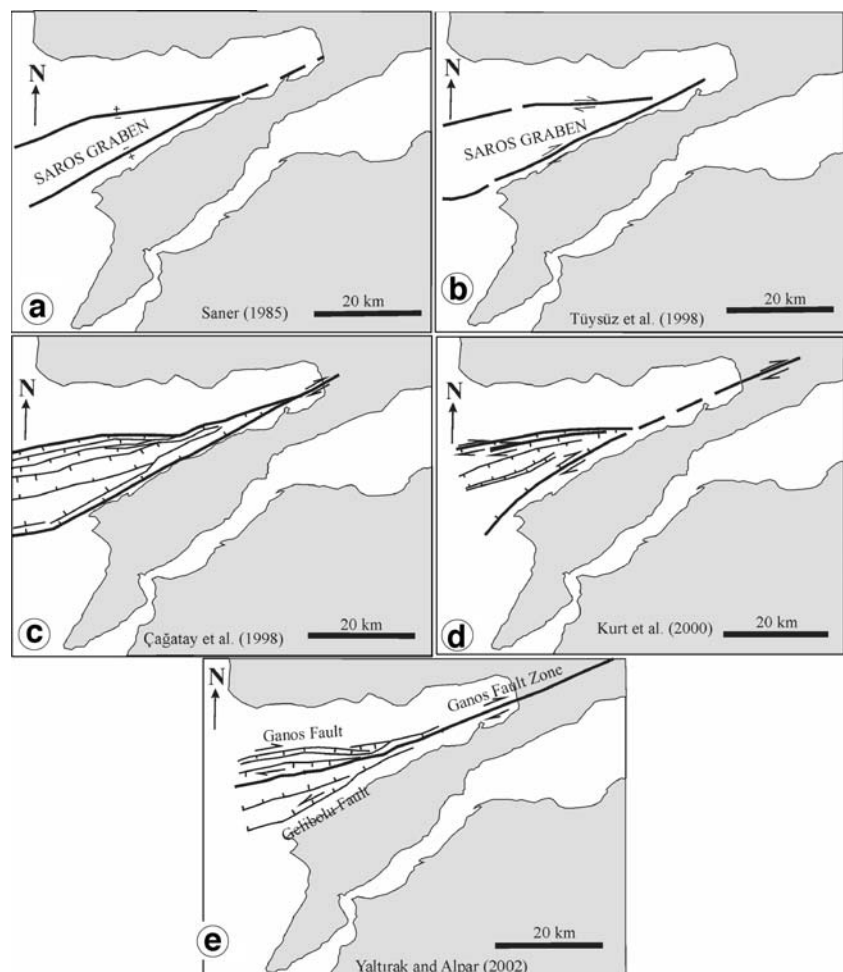
Debate also persists on the exact location of the Ganos Fault beneath the Gulf of Saros. Different fault maps based on seismic data have been produced for the Saros Gulf (Fig. 2). Some authors considered the Ganos Fault to bound the southern basin margin, others that the fault forms its northern margin, and yet others inferred that the fault splits up into several segments along the eastern edge of the gulf, thereby controlling both the northern and southern basin margins. The presence of some secondary faults along the basin floor was actually documented in some of these studies (Fig. 2c–e). A detailed geophysical study of the eastern North Aegean Trough and the western part of the Gulf of Saros, based on side-scan sonar data and sub-bottom profiler, was carried out by McNeill et al. (2004). They demonstrated the presence of Riedel-type structures accommodating dextral displacements in the central part of the basin. These are considered to coexist with the basin-bounding trans-tensional faults which control the vertical topography.

In this paper, we address the discrepancies regarding the active tectonics of the Saros Basin and the role of the NAFZ in its structural evolution. In particular, the hypothesis is tested whether the northern fault zone is the continuation of the Ganos Fault, and whether the southern fault zone formed to accommodate the NE-SW-trending extensional deformation imposed by the left-stepping nature of the Ganos Fault.

Geology and morphology of the Saros Gulf and surrounding areas

The stratigraphy of the land area surrounding the Gulf of Saros is dominated by early Eocene and younger sedimentary-volcanic successions (Fig. 1b). Four major unconformities have been determined in the Tertiary–Quaternary part of the stratigraphy, which constrain the timing of tectonic events in this area and the periods of erosion and subsidence (Saner 1985; Sümengen et al. 1987; Çağatay et al. 1998). These form the base of the mid-Eocene, late Miocene, Pliocene and Quaternary successions.

The Eocene to Oligocene units are exposed along the northern and southern coasts of the Gelibolu and Thrace peninsulas respectively (Fig. 1b). The unconformably overlying late Miocene units crop out on the slopes of the Gelibolu and Biga peninsulas along the Çanakkale Strait, and along the northern shores of the Gulf of Saros near the town of Enez at the Turkish–Greek border. The late Miocene sedimentary sequence shows some facies differentiations on the Thrace and Gelibolu peninsulas (Saner 1985; Sümengen et al. 1987; Tüysüz et al. 1998). Thus, the sequence was initially deposited in a fluvial and subsequently in a lacustrine environment on the Gelibolu

Peninsula, whereas marine sedimentation prevailed on the Thrace Peninsula over the same time interval (Sümengen et al. 1987). An upward-coarsening sequence of clastic deposits lies unconformably on the late Miocene sequence on the Gelibolu Peninsula, considered of Pliocene–Quaternary age (Fig. 1b; Erol and Nuttal 1973; Sümengen et al. 1987; Siyako et al. 1989; Tüysüz et al. 1998; Yaltırak et al. 1998; Şengör et al. 2005). Quaternary marine and fluvial terraces, and alluvial deposits of modern rivers constitute the Recent geology around the Saros Gulf (Fig. 1b).

The present morphology of the terrestrial areas around the Marmara Sea, including the Gulf of Saros, is governed by the cumulative effects of alternating erosion and tectonic processes since the early Miocene. A horizontal, mature erosion surface formed during the Pliocene. It was subsequently rejuvenated by tectonic activities and sea-level fluctuations during the Quaternary (Cvijic 1908; Pamir 1938; Gökaşan et al. 1997, 2005; Emre et al. 1998; Erinç 2000; Elmas 2003; Yiğitbaş et al. 2004; Yılmaz 2007). During the Quaternary, some parts of this mature surface were lowered below sea level by faulting and erosion, thereby defining a new base level for deposition (i.e. the Çanakkale Strait and Saros Gulf). The land area, on the other hand, was raised—a number of marine terraces of ages exceeding 250 ka are found as isolated remnants along the coast at different altitudes above the present sea level around the Marmara Sea, and along the western Black Sea coasts of Anatolia (Emre et al. 1998; Demirbağ et al. 1999; Yaltırak et al. 2000, 2002; Elmas 2003; Yiğitbaş et al. 2004; Gökaşan et al. 2005; Yılmaz 2007). The Thrace, Gelibolu and Biga peninsulas constitute the western elements of the elevated parts of this surface (Fig. 3).

Material and methods

Multi-beam bathymetric data were collected in 2005 from onboard the research vessels TCG *Çubuklu* and TCG *Çeşme* operated by the Turkish Navy, Department of Navigation, Hydrography and Oceanography (TN-DNHO). The Elac BCC Marko multi-beam system operates with 56 beams at 50 kHz. It has a range of 2,500 m, the fan of echo-sounders mounted below the survey vessels covering a total angle of approximately 120°. The horizontal coverage of the beams corresponds to three times the water depth. DGPS was used for positioning. The vessel speed was held at 8–10 knots.

A total of 560 km of high-resolution single-channel seismic data was collected in the Saros Gulf and the western offshore of the Gelibolu and Biga peninsulas from onboard the TCG *Çubuklu* during several cruises in 1995 and 1996 (Fig. 1b). An analogue spark array seismic system composed of a seismic energy unit (1,000 J), a transducer, a
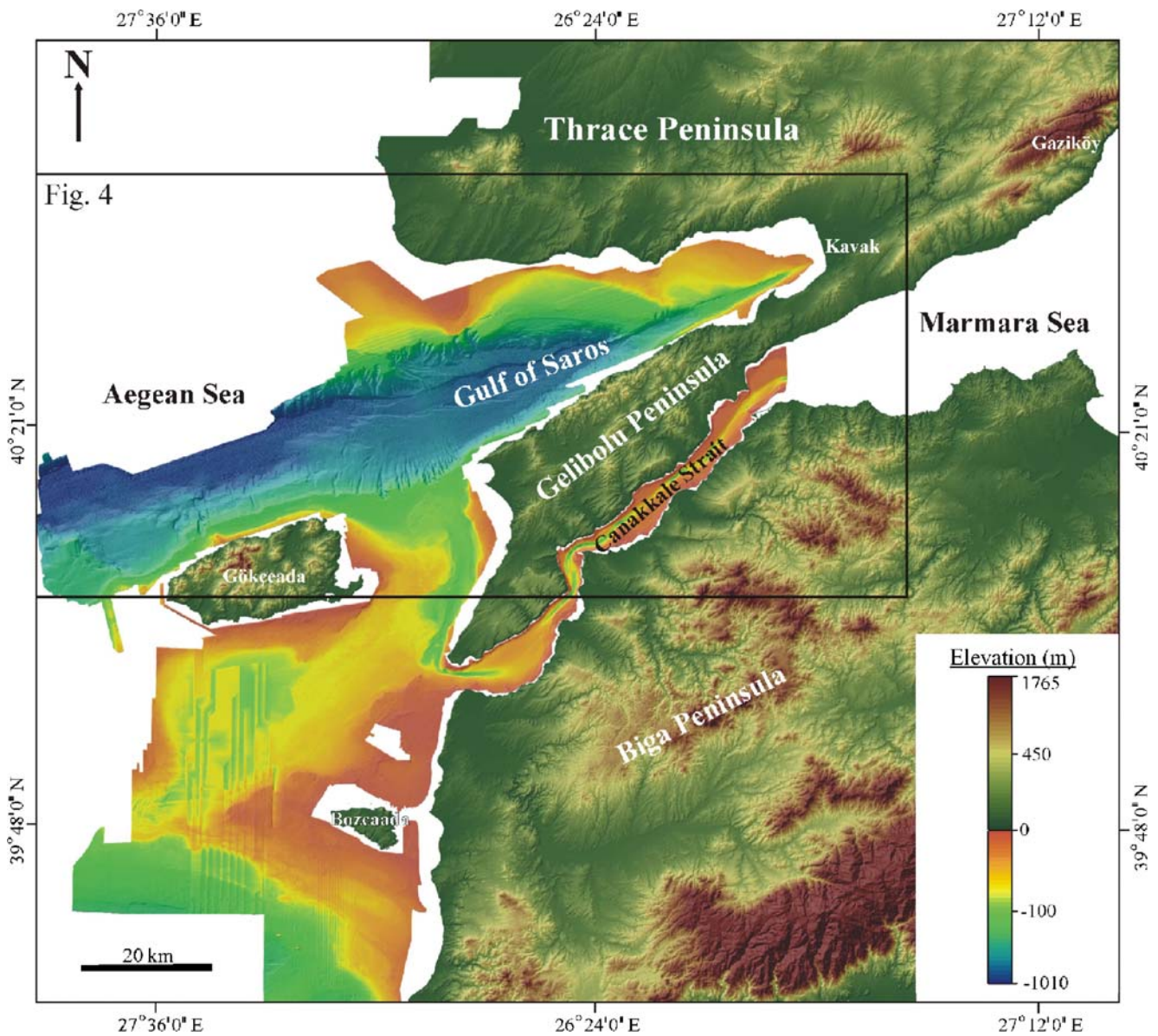
Fig. 3 Digital elevation model of the study area. The *box* indicates the location of Fig. 4

single-channel hydrophone streamer and an analogue recorder was used during the surveys. The ship speed was about 4 knots, and the recorder was set at 400-ms scan increments across the recording paper, the total depth coverage amounting to 1.2 s. Positioning was achieved by a Trisponder system. High-resolution seismic data previously interpreted by Çağatay et al. (1998) and by Yaltırak et al. (1998), and multi-channel seismic data collected and processed by Saatçılar et al. (1999) and Kurt et al. (2000; Fig. 1b) were geologically reinterpreted for this study in terms of the new swath bathymetric data.

A digital elevation model (DEM) was produced from 1/ 25,000 digital topographical maps and the multi-beam bathymetric data. These digital datasets were converted into raster maps with a pixel size of 20×20 m by means of

ArcGIS 8.3 software. The resulting DEM of the land area has a cell size of 20 m and a residual root mean square (RMS) of ±8 m. ArcGIS 8.3 was also used to merge and visualize the two datasets. The combined maps were then used for detail assessments of the morphological and morphodynamic character of the study area.

Results

Seafloor morphology

The swath bathymetry map clearly outlines the submarine features in the Gulf of Saros (Fig. 3). It consists mainly of a broad shelf along the north coast, and a deep trough along
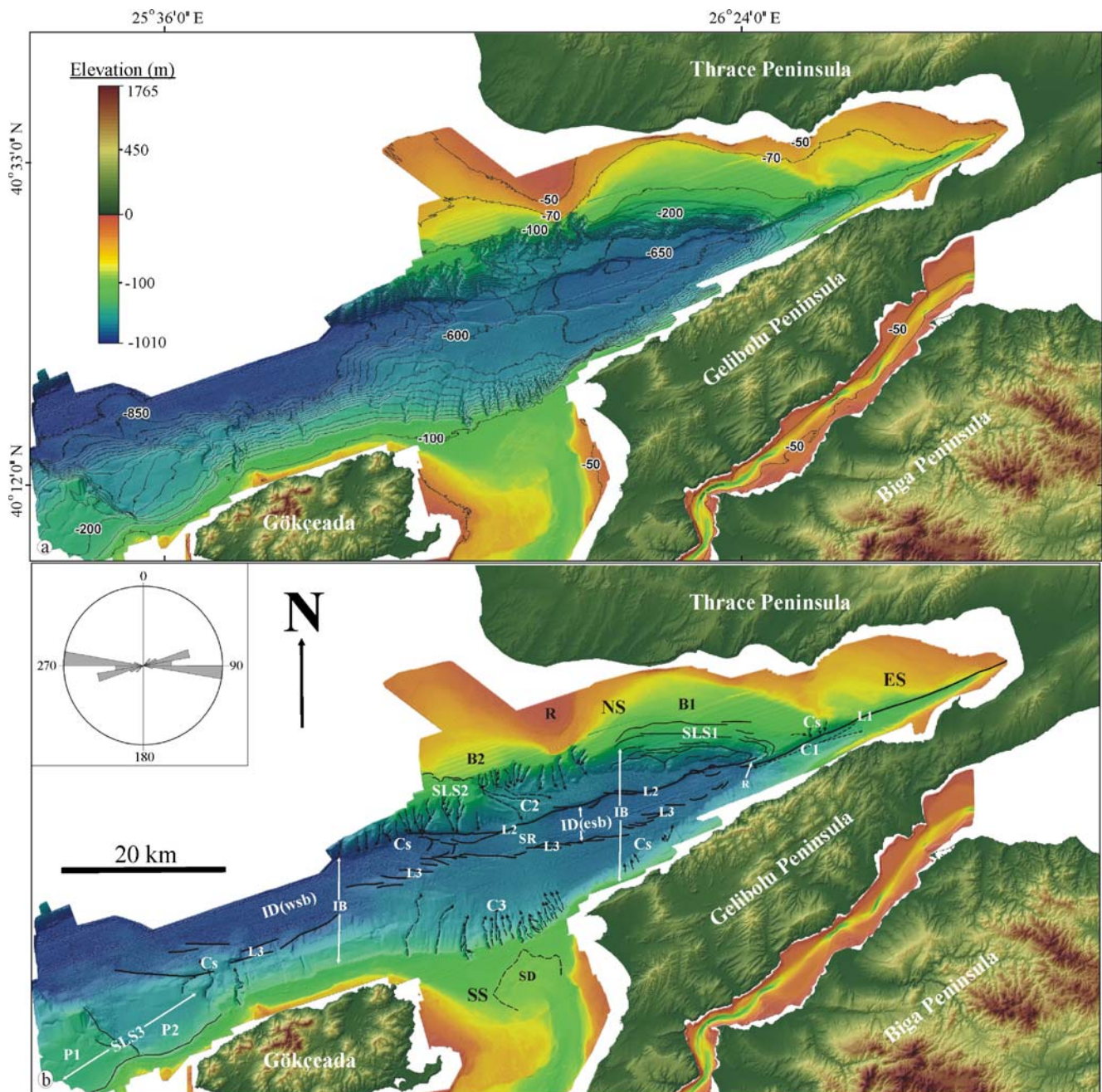
Fig. 4 a Bathymetry of the Saros Gulf. **b** Annotated digital elevation model of the Saros Gulf. *B* Basin, *C* canyon, *Cs* channel/canyon system, *ES* eastern shelf, *esb* eastern sub-basin, *IB* inner basin, *ID* inner depression, *L* lineament, *NS* northern shelf, *P* plain, *R* ridge, *SD* submarine delta, *SLS* submarine landslide, *SR* submarine ridge, *SS* southern shelf, *wsb* western sub-basin. The *inset* shows the rose diagram for the azimuths of the scars in the study area

the southern side off the Gelibolu Peninsula (Fig. 4). The northern shelf forms a broad plain between the Thrace shoreline and the −100 m bathymetric contour (Fig. 4a). It has an average inclination of 2.5°. The undulating −70 m bathymetric contour traces a slightly raised ridge on the shelf plain (Fig. 4a, b). The lower areas on either side of this ridge suggest the existence of subsiding basins (B1 and B2; Fig. 4a, b). Along the shelf edges of these basins (B1 and B2), several concave lineaments are observed which

correspond to small steps in the seabed (Fig. 4b). These steps are interpreted as the morphological expression of the fractures generated by two large submarine landslides (SLS1 and SLS2), and which are possibly still active today. A submarine plain in the eastern corner of the gulf appears to be the continuation of the northern shelf (towards the eastern shelf; Fig. 4). In this area, the eastern shelf is cut by a NE-SW-oriented, narrow linear canyon (C1; Fig. 4b) which connects the eastern corner of the gulf coast with the eastern

edge of the adjacent deepwater plain. The northern slope of this canyon is represented by a linear and vertical scar (L1), whereas the southern slope has a relatively smooth morphology. Two landslides are present on the northern slope. An elongated ridge appears where the canyon merges with the deepwater plain (ridge indicated by R on Fig. 4b).

The northern shelf break is characterised by a dramatic increase in slope (from 2.5° to 28°). The morphology of this northern slope is rather complicated, the chaotic structure being caused by numerous canyon incisions and by submarine landslides (Fig. 4). However, landslides SLS1 and SLS2 appear to be the most dominant features controlling the concave morphology in this region. A WNW-ESE-oriented, wide U-shaped canyon (C2) is located between these landslides (Fig. 4b). Several secondary canyon heads join the main axis and create a large erosional space along the central axis of the canyon, whereby the northern slope makes a left step. A ridge, possibly formed by sediments, is situated at the base of the erosional space (Fig. 4a). Several secondary canyons are cut into the sedimentary ridge (Fig. 4b).

The southern slope of the gulf, by contrast, is more linear and incised by fewer canyons (Fig. 4b). A group of canyons (C3) occur where the linear slope becomes indented between the Gelibolu Peninsula and Gökçeada Island (Fig. 4b). These canyons are related to the submarine extension of the Çanakkale Strait which ends in a submarine delta on the southern shelf.

Along the southern slope of the gulf, north of Gelibolu Peninsula (Fig. 4), a proper shelf is not developed, whereas a wide shelf is again present between the Gelibolu Peninsula and Gökçeada. North of Gökçeada, the shelf becomes narrow once more (Figs. 3 and 4). The two submarine plains northwest of Gökçeada (P1 and P2) represent the upper surfaces of slide blocks associated with a large submarine landslide (SLS3; Fig. 4b).

The floor of the Saros Gulf basin consists of two sub-basins separated by a submarine ridge (SR) located between the canyons C2 and C3 (Fig. 4a, b). Whereas the depth of the eastern sub-basin (esb) reaches down to −700 m, the western sub-basin (wsb) reaches ca. −850 m (Fig. 4a, b). The most prominent morphological feature in the Gulf of Saros, however, is a NE-SW-oriented depression, the so-called inner depression (ID; Fig. 4a, b). The remainder of the basin floor on both sides of the depression consists of elevated flats which form the flanks of the ID (Fig. 4), and which have up to 100-m-high steep slopes on their northern and southern sides (marked as L2 and L3 respectively on Figs. 4 and 5). The northern margin of the inner depression is marked by a continuous but curved scar which resembles large corrugations on fault planes. This margin can be subdivided into E-W- and NE-SW-trending segments. The E–W segments seem to be older structures connected to

each other by the NE-SW-trending segments. West of the submarine ridge (SR on Fig. 4b), the length of the E-W-trending segments exceeds 10 km, whereas to the east they vary from 3 to 4 km in length. The lengths of the NE-SW-trending segments are 7–8 km on average (Fig. 5a).

In contrast to the northern margin, the southern margin of the ID is not marked by a continuous scar. Instead, it is formed mostly by E-W-oriented en-echelon fractures similar to synthetic Riedel shears, separated by NW-dipping smooth slopes (Fig. 5b). The NW-SE-trending en-echelon fractures shape the southern margin of the ID to the NW of Gökçeada, whereas these fractures approximately align in an E–W direction in the Gulf of Saros. As in the case of the northern margin, two trends are also recognisable along the southern margin of the ID, i.e. NE-SW- and E-W-trending segments. The en-echelon fractures are isolated and widely spaced in the NE–SW segments, but are more closely spaced and even coalescing in the E-W-trending segments. The E-W-trending fractures cut and dextrally offset the NE-SW-trending segments and thereby shape the southern margin. Lateral offsets along these fractures decrease from 5 to 1–2 km in the SW–NE direction. Vertical offsets in these E–W fractures decrease from southwest (>90 m) to northeast (<35 m), causing the southern margin of the inner depression to gradually disappear towards the east (Fig. 4b).

The closely spaced Riedel fractures in the E–W segments along the southern basin margin generate a group of southward-tilted fault blocks (Fig. 6). Here, the vertical offsets decrease from the western towards the eastern tips of the individual Riedel shear fractures. NW–SE-striking shear fractures are rotated towards the NE–SW by bending the tips of the individual faults in this zone (Fig. 6). Along both margins of the ID, the mean strike of the E-W-oriented scars varies from 90° to 95°, whereas the NE-SW-oriented scars strike approximately 70° (inset of Fig. 4b).

The northern and southern margins of the inner depression bend towards each other and merge in the east, thus delimiting the ID there. The lineament L1 first appears between the tips of the merged northern and southern margins of the ID along the eastern edge of the eastern sub-basin, cuts through the slope and platform of the eastern shelf, and then runs towards the shore (Fig. 7; cf. also Figs. 4b and 5).

Seismic stratigraphy

The seismic stratigraphy of the Saros Gulf, calibrated by means of dated gravity cores and borehole data from the northern shelf, has previously been studied by Çağatay et al. (1998). They showed that late Quaternary sediments, which unconformably overlie a folded late Miocene basement on the northern shelf, can be subdivided into three units: an older marine unit (<50 m thick), an overlying
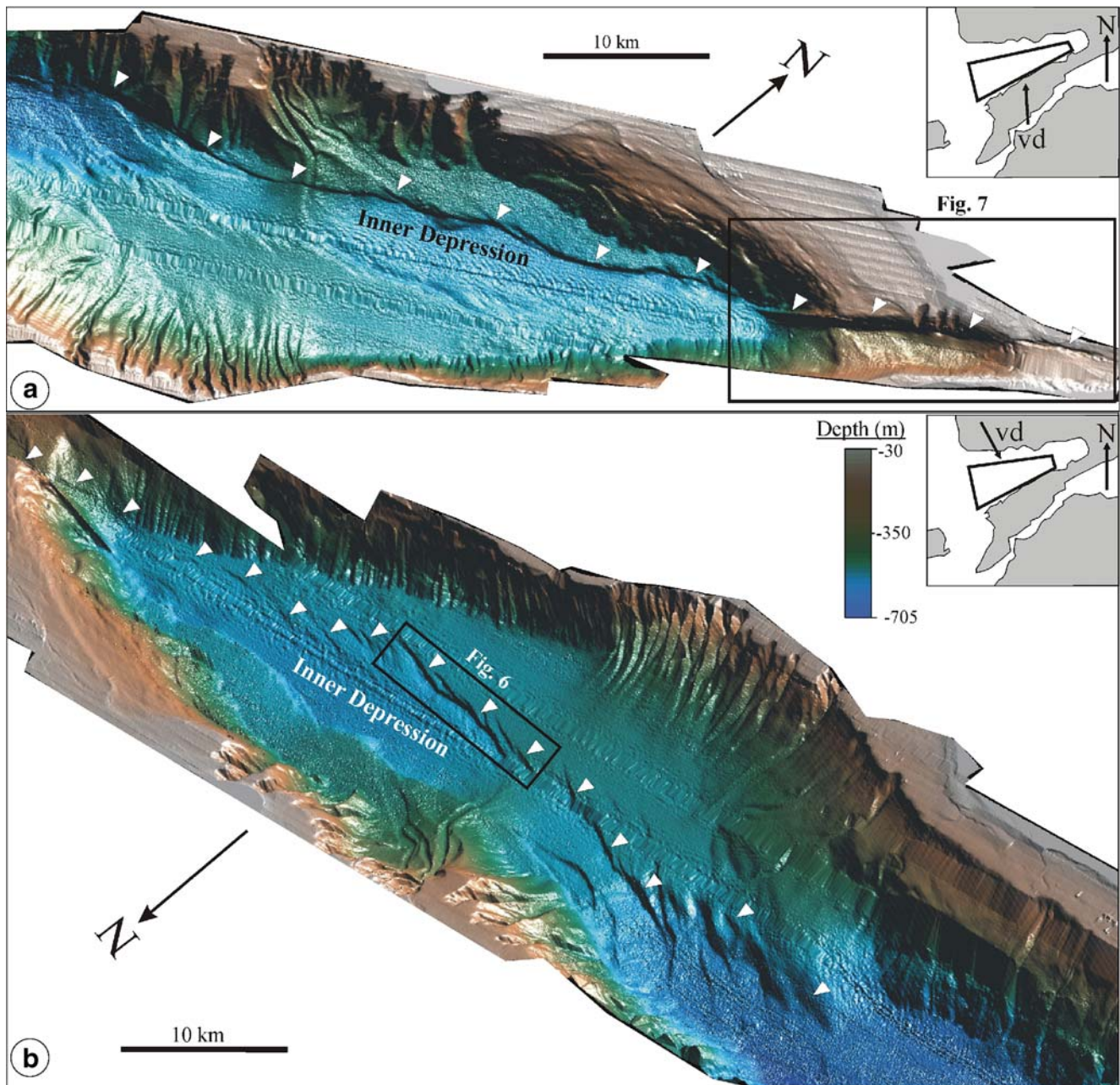
Fig. 5 Digital elevation models of the Saros Gulf under different light directions (in the *insets*, *vd* denotes view direction), showing the lineaments. **a** L1 and **b** L2

prograding delta (25–13 ka, 40 m thick), and an upper marine unit (<13 ka, <20 m thick). The oldest sediments are inferred to be <200 ka in age (deposited during the Riss–Würm interglacial stage; Çağatay et al. 1998). Çağatay et al. (1998) followed this stratigraphy through to the so-called inner basin, the inner depression, and the southern shelf.

The data from the northern shelf indicate that up to a maximum of 110 m of sediments was deposited over the late Miocene basement units during the late Quaternary–Holocene period, Pliocene deposits being absent (Çağatay

et al. 1998). The total thickness of the sediments in the inner depression, on the other hand, exceeds 1,500 m, according to the deep seismic profile illustrated in Fig. 8. There are no borehole data for the inner depression, and the age of this succession is therefore essentially unknown. According to the interpretations of Çağatay et al. (1998), the uppermost 110 m of this succession is late Quaternary. The thickness of the sediments thus remains constant on both shelves, in the inner basin, and in the inner depression.

The sediments deposited in the inner basin can be subdivided into four seismo-stratigraphic units, termed BD1
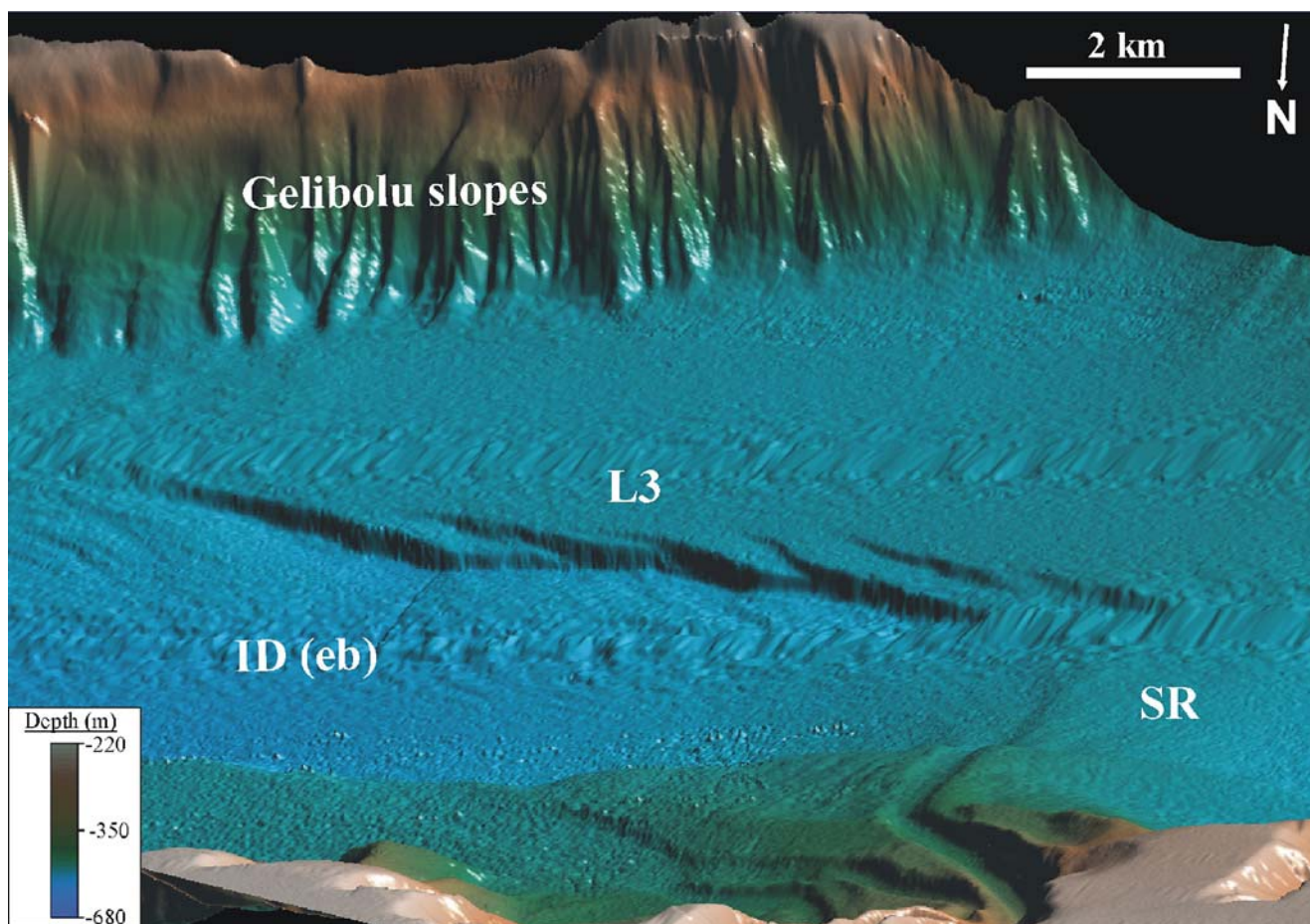
Fig. 6 Three-dimensional diagram of the inner basin, showing details of lineament L3. In this area, L3 is represented by five closely spaced, synthetic Riedel fault blocks. Each fault block is tilted southwards. The vertical offset increases westwards from 0 to ca. 60 m along each fault, and thus generates a relay ramp on the fault blocks. NE-SW-trending faults cut the relay ramps, and link the two neighbouring Riedel faults. Note that the eastern tips of some faults bend sharply and align in an E–W direction. Details of the canyon (C2) and the submarine ridge (*SR*) are also visible. *eb* Eastern sub-basin, *ID* inner depression

to BD4 (Fig. 8). Sediments marked BD4 to the south of L3 onlap onto the low-angle upper surface of the basement. Also the seismic units marked BD1 to BD3 terminate with onlaps onto the steeply sloping basement on the same profile (Fig. 8). Some faults are present in unit BD1, which is unconformably overlain by unit BD2 near the southern margin of the inner basin. These are the oldest faults in the inner basin. Another fault exists further south, cutting the units BD1, BD2, and the lower part of BD3. This fault evidently became inactive before the uppermost part of BD3 was deposited.

No structural break can be observed between the inner basin and the northern slopes of the southern shelf on this seismic profile (Fig. 9; cf. also Fig. 8). Behind the southern slope, a south-facing reverse fault has been identified near the shelf break to the west of the Gelibolu Peninsula, even though this part of the profile is affected by strong multiple reflectors (Kurt et al. 2000; Fig. 8). This fault seems to have been inactive for some time, as it is buried by the most recent shelf sediments. It is thought to have been responsible for the uplifting of the Gelibolu Peninsula (Yaltırak et al. 1998; Yaltırak and Alpar 2002).

The late Miocene and late Quaternary units on the shelves can be distinguished from each other by the state of their deformation. Thus, the late Miocene units are folded on both shelves, whereas the overlying Quaternary units are represented by flat and relatively non-deformed seismic reflectors (Çağatay et al. 1998). Such deformed units do not occur in the inner basin. Instead, the reflectors of the ID units are generally similar, except for BD1 which shows faulting-related deformation at the basin margin. In view of its deformed nature, BD1 is probably of Pliocene age, the remainder of the deposits thus being considered to be Pliocene–Quaternary.

Active faulting in the Gulf of Saros and the NE Aegean Sea

Previously published seismic profiles were used to check whether the northern margin of the inner depression and the lineament L1 described above are structurally controlled. In
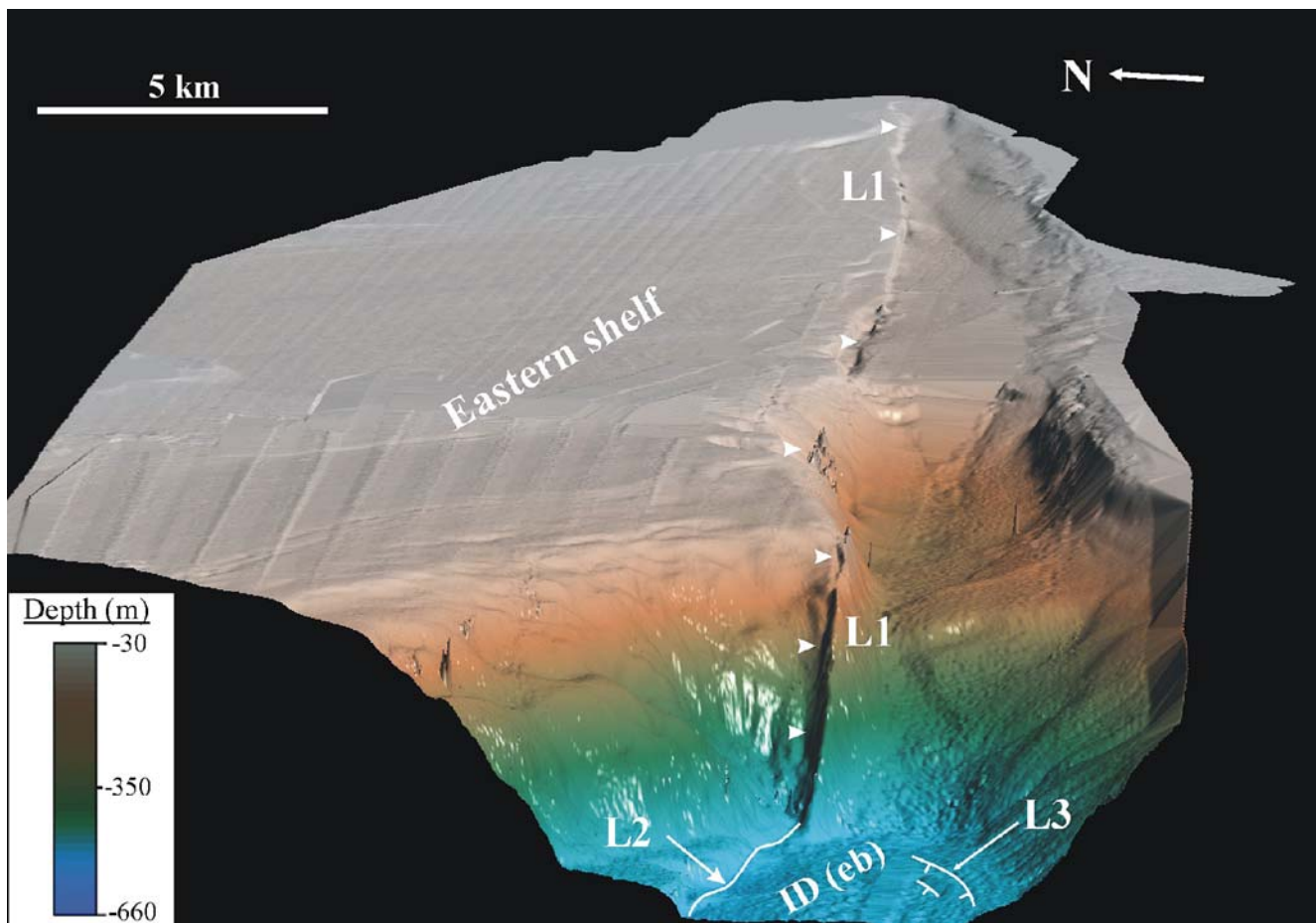
Fig. 7 Three-dimensional diagram showing the morphology and structure of the eastern shelf, lineament L1, and the eastern edge of the inner depression (*ID*; *eb* eastern basin). L1 ends abruptly at the edge of the inner depression, dipping northwards at high angles, suggesting that it incorporates a reverse component. The fresh scar is suggestive of a recent rupture along L1. Note that some sediment covers this scar at the edge of the eastern shelf, where two landslides are also present. Lineament L2 starts adjacent to L1, but lineament L3 is hardly visible due to the smaller vertical offsets. Landslide scars affecting the northern and eastern shelf are also visible (*lower left*)

Fig. 10, a seismic section cutting both the northern (L2) and southern (L3) margins of the ID, both the northern and southern slopes of the inner basin, and the northern shelf is shown. A major submarine landslide along the edge of the northern shelf (SLS2) is characterised by chaotic reflectors and slip surfaces (inset A of Fig. 10; cf. also Fig. 4b). The northern margin of the ID (L2) is marked by two parallel vertical faults (inset B of Fig. 10). The southern fault corresponds to the northern margin proper of the ID, whereas the northern fault is one of the secondary, cross-cutting NW-SE-trending shear zones (inset B of Fig. 10). The L2 faults thus appear to be of tectonic origin. The motion along the L2 fault planes has generated a ca. 100-m vertical offset in the seabed. The seabed of the ID dips at low angles towards the northern margin (L2) on this profile. The sedimentary fill also dips northwards at low angles, but the angle of dip increases adjacent to the basin margin fault to generate an asymmetrical anticline. The sedimentary sequences of the northern fault block, on the other hand, dip southwards with a low angle inclined towards the L2

faults (inset B of Fig. 10). It is not clear from this profile whether the vertical component is related to compression or extension, since no distinct dip of L2 can be recognised. The en-echelon Riedel fractures marking the southern margin of the ID are represented by three parallel faults on inset B of Fig. 10. Again, the folding of the sedimentary sequence in these fault blocks suggests that both vertical and lateral (dextral in this case) shearing occurred along these.

The seismic profile in Fig. 8 cuts the Gulf of Saros obliquely in a NE–SW direction, and incorporates all the components of the basin system described above (Kurt et al. 2000). The northern margin of the ID is marked by a single fault (L2, Fig. 8), whereas the southern margin is represented by four faults (L3). The L2 faults seem to be vertical with a steep dip towards the north, i.e. towards the base. The southernmost fault in L3 is the most prominent one, cutting the stratigraphic sequence vertically to a depth of at least 1.7 s, whereas the other faults in this group dip northwards with steep angles, and remain as shallower
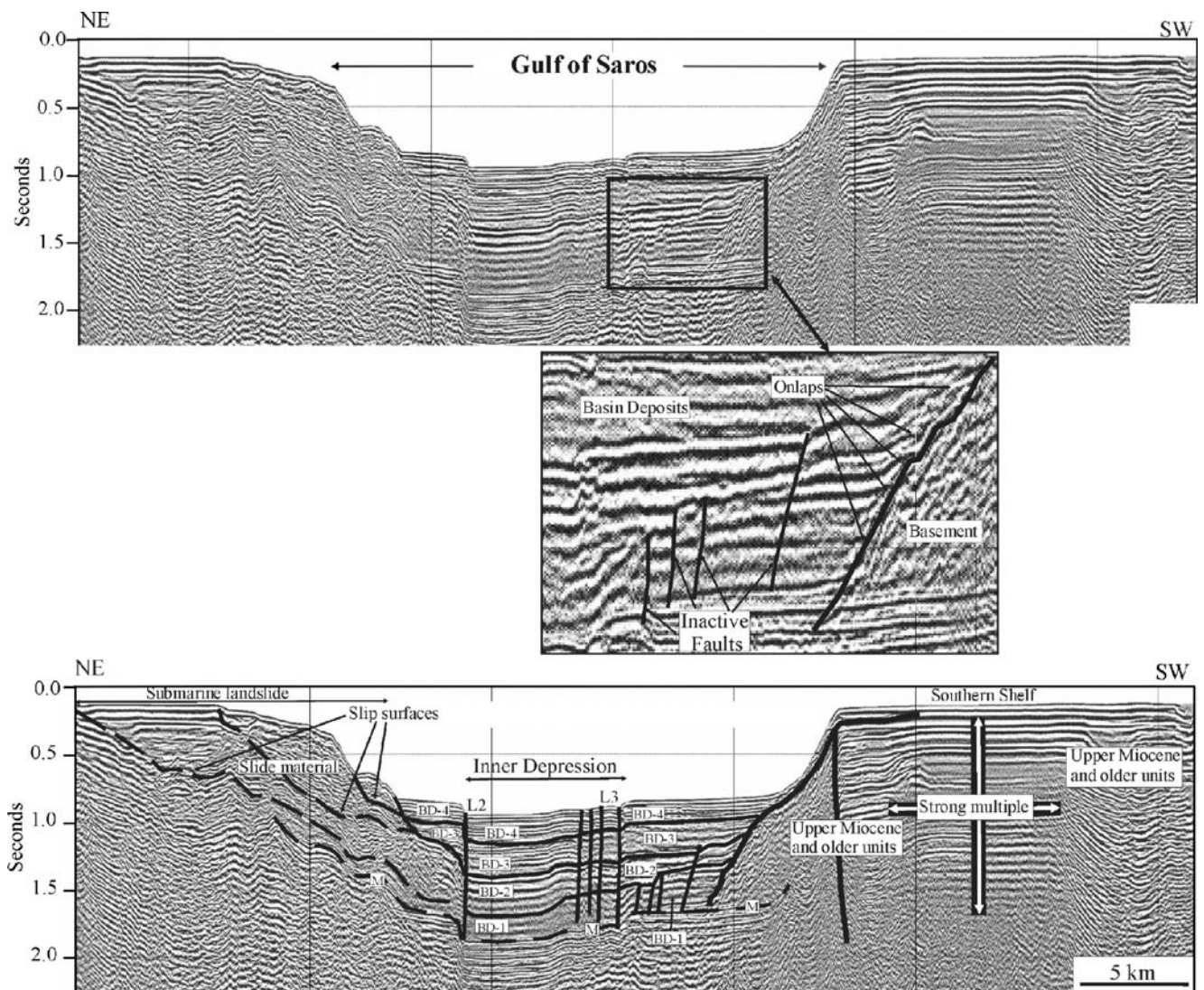
Fig. 8 Original (*top*) and interpreted (*bottom*) multi-channel seismic profile from the Saros Gulf (see Fig. 1b for location, and text for explanation). *BD* Basin deposits, *M* multiple

structures penetrating to a depth of <1.3 s. An anticline is present to the immediate north of L3 along the southern margin of the inner depression. This is likely to be an active structure which still shapes the seafloor today.

The northern slope of the inner basin is dominated by the submarine landslides visible in Fig. 8. Mass-wasting along the northern shelf edge is apparent here, in the form of three different landslides. All these landslides are unconformably overlain by the units BD3 and BD4 to the north of L2, which also cut and thereby delimit the landslides. Extensions of these landslides into the inner depression can not be detected on the seismic profile of Fig. 8.

The seismic profile illustrated in Fig. 9 cuts the northern shelf, L1 and the northern slope of the Gelibolu Peninsula. No deformation affecting the basin deposits and the seabed along the boundary surface between the basin deposits and basement is evident (Fig. 9). Instead, the basin deposits

onlap onto the northern slope of the Gelibolu Peninsula, suggesting that the contact of the slope with the basinal deposits is stratigraphic, not tectonic in origin. On this profile, L1 appears to be a major vertical fault which intensively deforms the basinal deposits, in the form of relatively tight folds. At the eastern corner of the Saros Gulf, L1 aligns with the surface rupture of the Ganos Fault located between the towns of Kavak and Gaziköy (Fig. 11; cf. also Fig. 7). Thus, the NE-SW-oriented L1 in the Saros Gulf represents the submarine extension of the Ganos Fault and, as such, is the westernmost extension of the dextral NAFZ.

The swath bathymetric and seismic data have revealed that the lineaments L1, L2 and L3 are the only active faults cutting the basin floor and slopes. L1 and L3 appear to be dextral strike–slip faults with some oblique components. Both dip–slip and lateral motion also occurs along L2 but the sense of the lateral shearing is not obvious. Morpho-
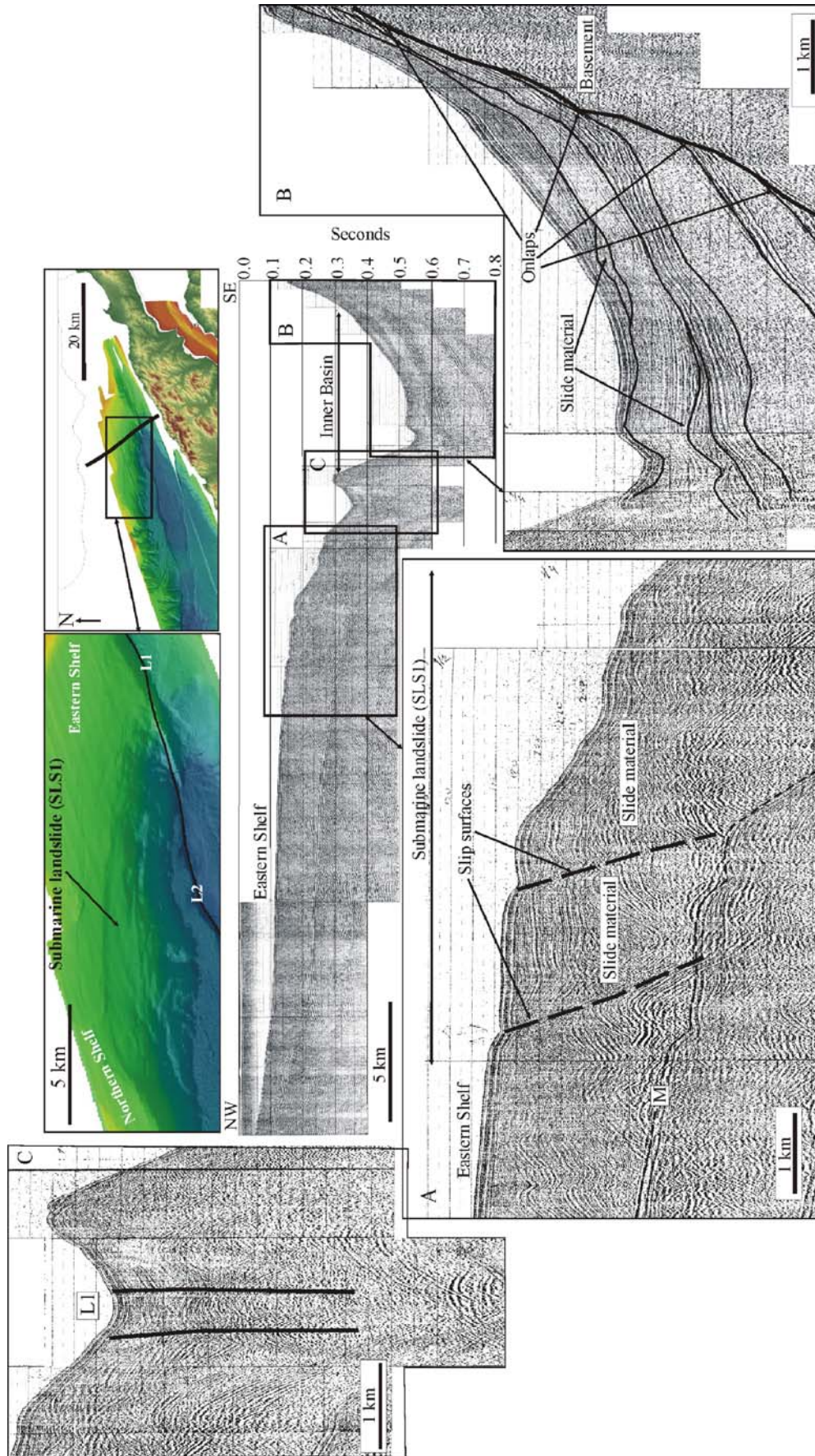
Fig. 9 High-resolution shallow-seismic profile and the eastern portion of the swath bathymetry of the Saros Gulf, showing the location of the submarine landslide (SLS1) affecting the northern and eastern shelf, as well as the location of the seismic profile. The slip surfaces of the landslide on the seismic profile were previously interpreted as normal faults, due to the absence of swath bathymetry data. *L* Lineament, *M* multiple
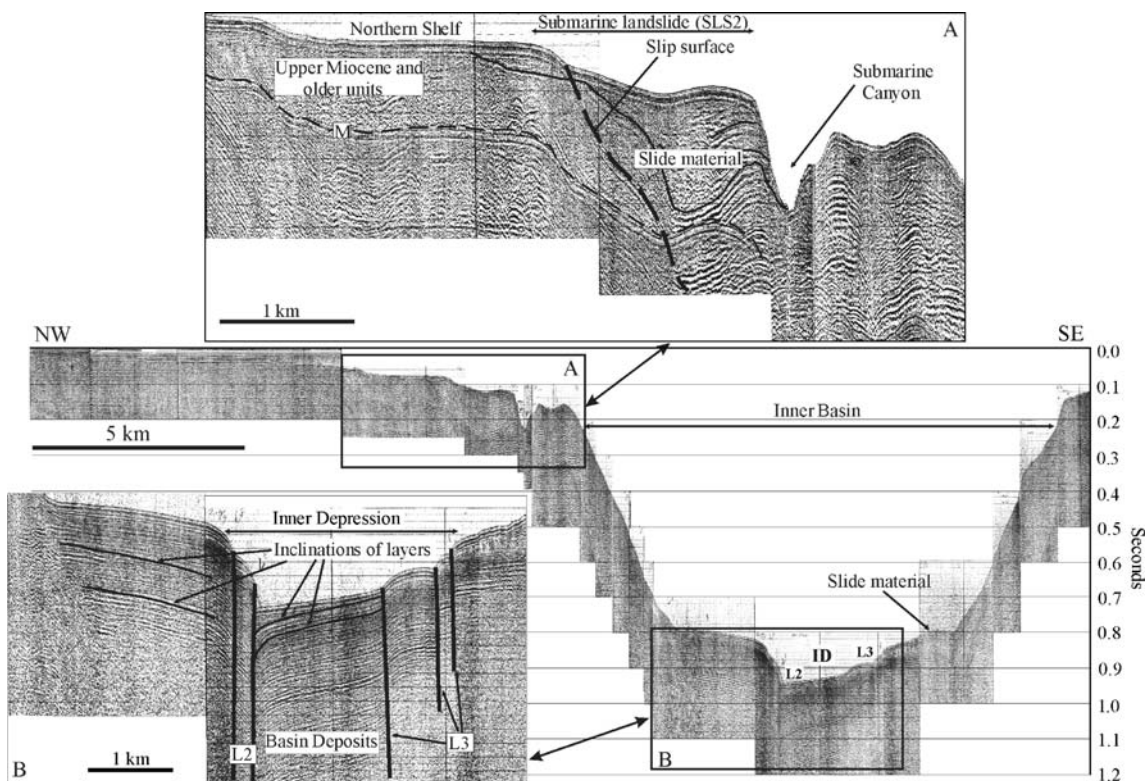
Fig. 10 High-resolution shallow-seismic profile from the Saros Gulf (see Fig. 1b for location and text for explanation). *ID* Inner depression, *L* lineament, *M* multiple

logical markers are rare across L2; the channel creating the deep-sea fan (DSF1) in the inner depression being the only marker available (Fig. 12). There is, however, no obvious lateral offset in this channel on either side of L2, although smaller offsets may not have been detected due to

resolution problems in swath bathymetric data analyses at larger scales. Another smaller fan (DSF2) occurs to the east of DSF1 and in front of L2, but it is not connected to any channel to the north. This proves the lateral offset along L2, but again the sense of shearing is not clear.

Fig. 11 Digital elevation map of the Thrace, Gelibolu and Biga peninsulas, showing the trace of the onland Ganos Fault. The map was prepared by using 1/25,000-scaled digital topographic data. The mountain range to the north of Gaziköy is termed the Ganos Mountains. It is interpreted as a push-up ridge formed by transpression due to a bend in the direction of the Main Marmara Fault (Okay et al. 2004) from E–W (Marmara Sea) to NE–SW (Gelibolu Peninsula)
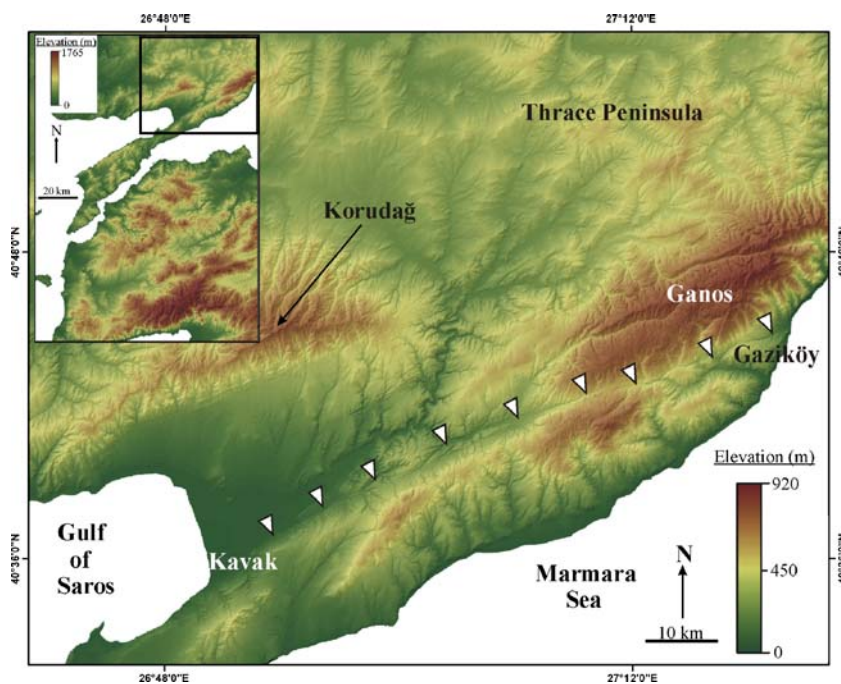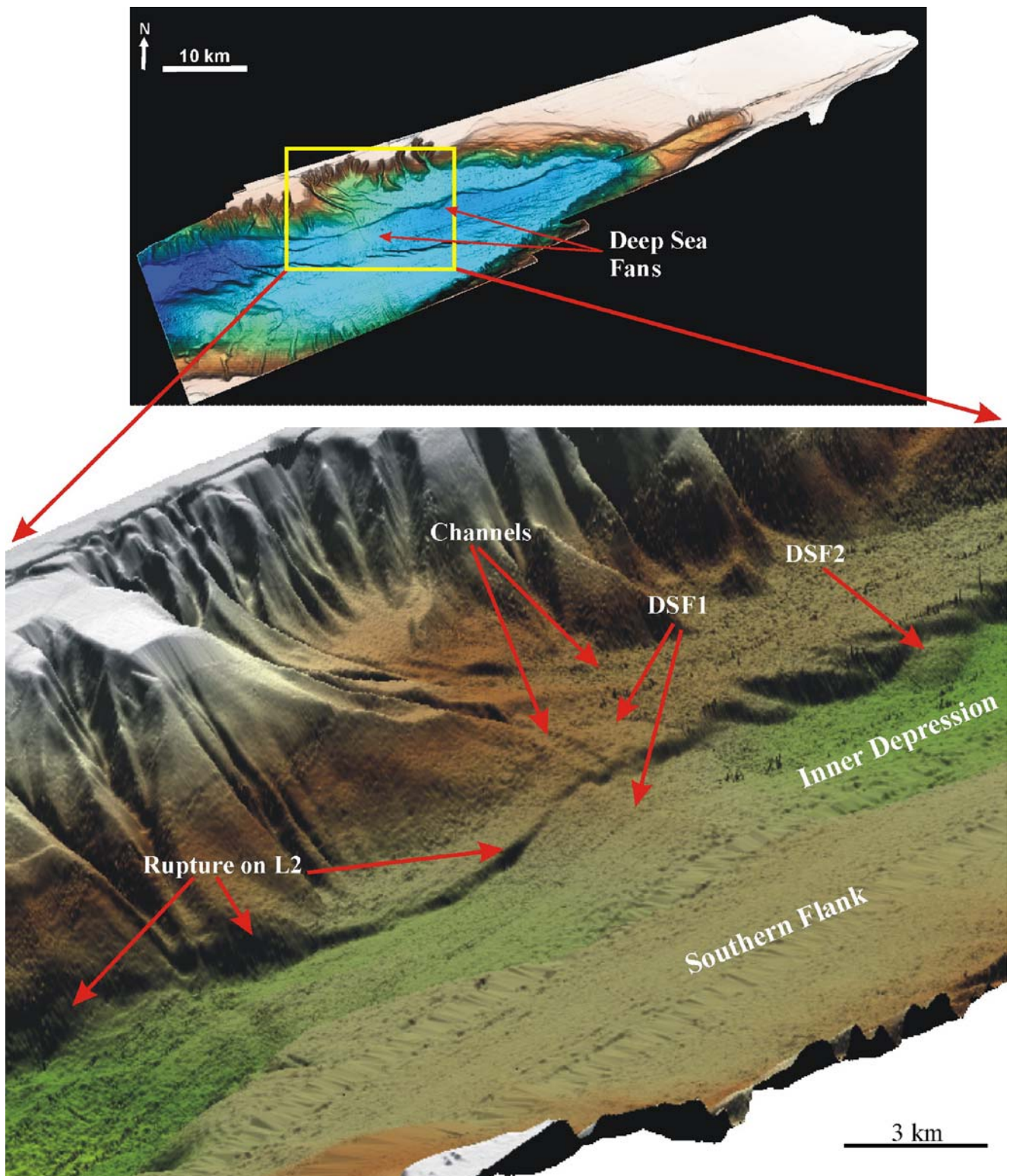
Fig. 12 Three-dimensional block diagram showing the morphology of the flanks of the inner depression. No apparent offset is detected on lineament L2 across the submarine ridge formed by deep-sea fan DSF1. DSF2, however, has no connection to any of the channels in this area, suggesting that the lateral offset occurred on L2. The *upper diagram* shows the location of the three-dimensional diagram (see text for explanation). *DSF* Deep-sea fan

Fig. 13 **a** Epicentre distribution and fault plane solutions of recent earthquakes under the Gulf of Saros and the NE Aegean Sea (compiled from Taymaz et al. 1991; Karabulut et al. 2006). **b** Earthquake activity in NW Turkey and the northern Aegean region. Note the location of the seismic gap or low-seismic activity zone in the Gulf of Saros and the Ganos Mountains area
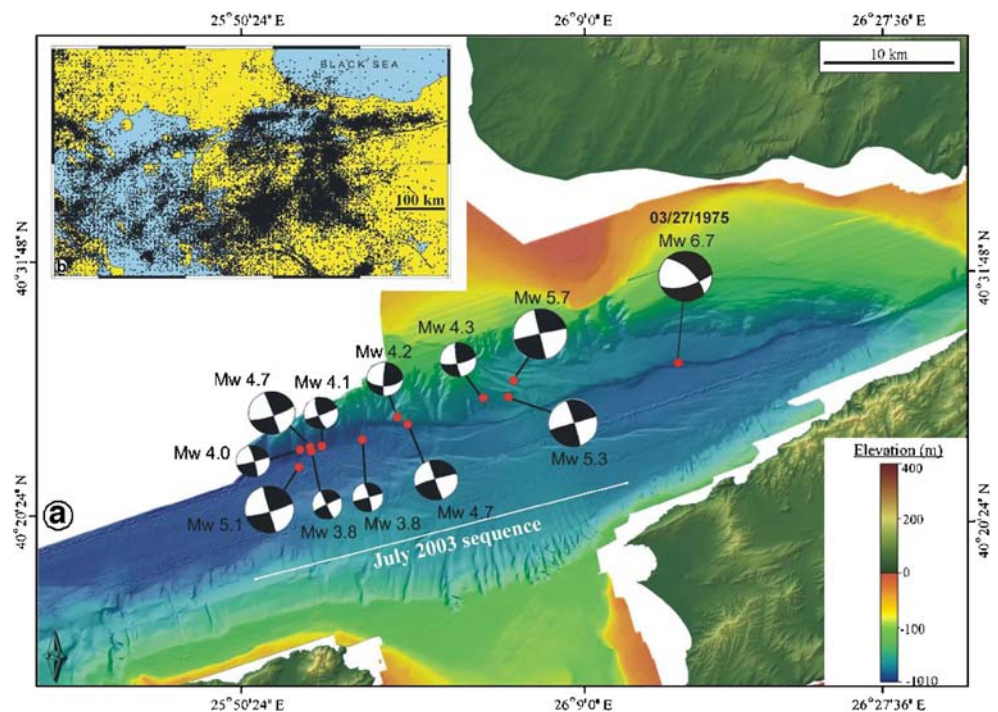
Useful information on the sense of shearing along the active faults in the Gulf of Saros can also be gleaned from the available seismological data. The Gulf of Saros is located along a 100-km-long seismic gap lying between the intensely active zones in the North Aegean Trough to the SW and the Marmara Sea to the NE (Karabulut et al. 2006; Fig. 13b). Figure 13a shows the epicentres and focal mechanism solutions of the July 2003 earthquake sequence (Karabulut et al. 2006) and the March 1975 event (Taymaz et al. 1991), which occurred at the western tip of the seismic gap. The epicentres of these earthquakes are mostly located on L2, only a few to the north of it. The depths of the hypocentres vary from 9 to 20 km, and most of the solutions indicate pure dextral slips with some oblique movements. It is thus clear that L2 is located at least 9 km above a pure right-lateral strike–slip fault zone. Due to the shallow penetration of the seismic profiles (1.7 s), it is not clear whether L2 and/or L3 coalesce downwards to merge with this seismic fault.

Active mass-wasting and deposition

Swath bathymetry and digital topography were combined to examine the source areas and sedimentation pattern within the Gulf of Saros and the eastern North Aegean Trough (Fig. 14). The land area surrounding the Gulf of Saros is characterised mostly by a mature erosional surface with some rejuvenation along the Ganos Fault in the east and northeast. The terrestrial drainage in the N and NE is directed towards the Gulf of Saros, whereas the main drainage on the Gelibolu Peninsula is towards the Strait of

Çanakkale (Gökaşan et al. 2007). Two channels (C1 and C2) are seen cutting the shelf along the northern and eastern shelves of the Gulf of Saros. This indicates that, at present, most of the sediments supplied by local rivers are trapped on the shelves, and only a limited amount is transported into the deep basins via these channels. The southern shelf between Gökçeada and the Gelibolu Peninsula is also cut by a channel (C3), which appears to be the submarine extension of the Strait of Çanakkale. This channel sharply bends from an E–W to a N–E direction at the Aegean Sea exit of the Çanakkale Strait before it bends to a NW–SE direction, in alignment with the western coastline of the Gelibolu Peninsula (Fig. 14). This narrow channel reaches the shelf break immediately west of the Gelibolu Peninsula (Kemikli Point), and probably transports sediment to the deep basin via a few canyons cut into the steep slope in front of it. As noted above, some sediments are trapped on the shelf in a submarine delta (SD) located above the shelf break. A number of other channels are present along the shelf break and on the steep slopes of the basin margins (Fig. 14; cf. also Fig. 4b). These channels seem to be the most prominent sediment transport routes into the inner basin and the cross-cutting inner depression.

At the distal tips of these channels, several deep-sea fans can be seen, located along the southern margin of the deep, western sub-basin of the ID to the N and NW of Gökçeada (Fig. 14). The same applies to the plain in front of the landslides on the northern shelf north of L2.

Another mechanism providing sediment to the ID is landsliding on both the northern and southern slopes. Besides the landslides along the northern shelf described
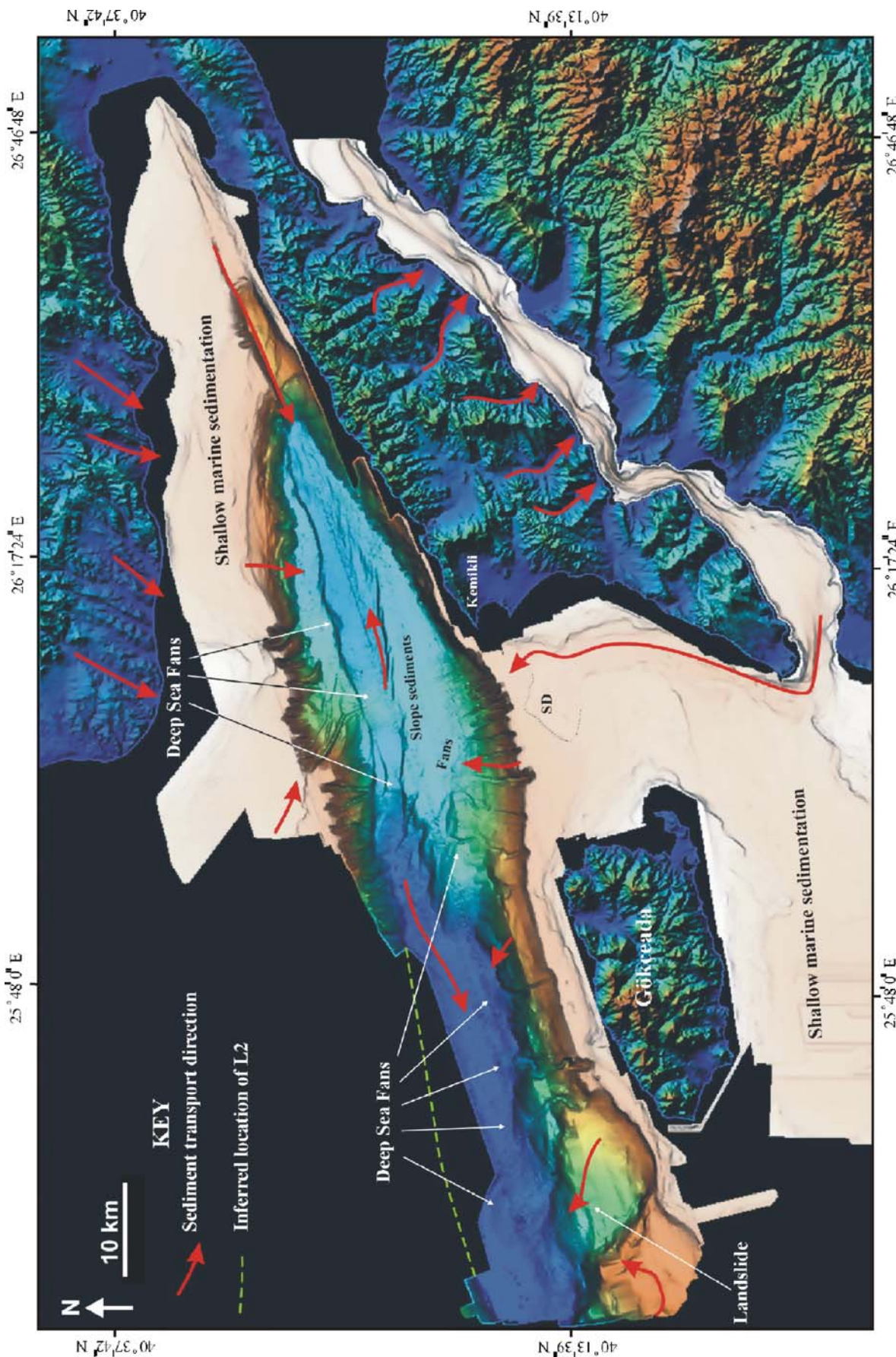
Fig. 14 Digital elevation model of the study area, showing the sediment transport directions from the land towards the adjacent marine areas. The N-S-trending (*red arrows*) at the exit of the Strait of Çanakkale is based on the study of Bayhan et al. (2001). Most of the sediments supplied from the land are considered to be deposited in shallow-marine areas, only a limited amount of continental sediment reaching the inner basin. However, a number of channels/canyons erode the slopes of the basin, and transport material to the deep basin. Note that a series of deep-sea fans are formed in front of such channels. The landslides are also important sediment sources for the inner basin. Both channel erosion and landsliding widen the basin continuously. *L* Lineament, *SD* submarine delta
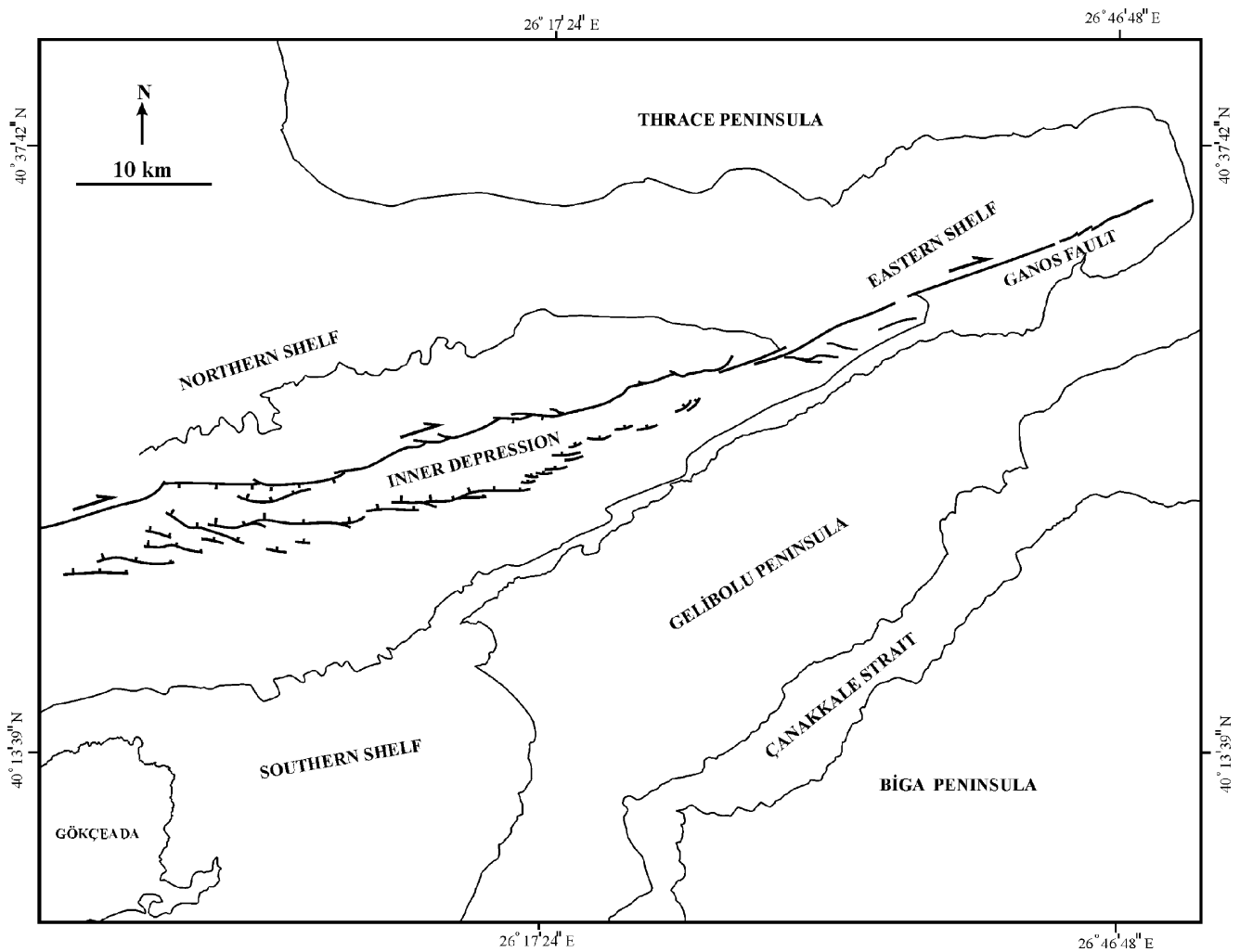
Fig. 15 Active fault map of the study area (see text for explanation)

above, a large landslide also exists to the NW of Gökçeada Island. This landslide is located immediately east of a NW-SE-trending, left-lateral strike–slip fault which lies beyond the present study area (McNeill et al. 2004). The western margin of this landslide runs parallel to the strike of this left-lateral fault.

As demonstrated above, there are two superimposed basins in the study area, i.e. the younger inner depression and the older inner basin. The faults bordering the ID produced additional tectonic subsidence in the basin system. Sediments bypassing the smooth slopes of the inner basin have been deposited in this newly formed accommodation space since its formation.

Discussion

Detailed analyses of the multi-beam bathymetric and seismic data presented above have shown that a deep-sea basin with over 1,500 m of sediment fill is present in the Gulf of Saros and the Northeast Aegean Sea. The basin is bordered by a wide shelf to the north and east, and a narrow shelf to the south. The steep slopes and the shelves of the basin are subject to mass-wasting, as revealed by the presence of large landslides and a number of channel/canyon systems. A series of deep-sea fans, formed at the base of the slopes of this basin, are indicative of high present-day sedimentation rates. Two active fault systems dissect this deep basin, and have generated an inner depression. The spectacular structures along the bounding fault zones make this area a unique natural laboratory for analogue modelling.

Interpretation of seismic structures

The structural map of the Gulf of Saros and the North Aegean Trough, as revealed on the swath bathymetry and the seismic profiles, is shown on Fig. 15. Contrary to previously

published structural maps (cf. Fig. 2), our study has shown that active faulting is confined to a narrow zone in the centre of the Gulf of Saros and the NAT. There are indeed some faults along the northern margin of the Gelibolu Peninsula, but these are inactive, since they do not penetrate up to the seafloor, being unconformably overlain by the upper part of BD3 and BD4. These presently inactive faults were responsible for tectonic subsidence during the initial formation of the inner basin. Overall, the active structures in the study area resemble those of a typical NE-SW-trending dextral shear zone. The most prominent structures are the combined L1 and L2 fault systems, which are part of a single major break-through fault.

Lineament L1 is interpreted to represent the submarine extension of the Ganos Fault (Fig. 15). The total length of this submarine segment of the Ganos Fault is 40 km. L1 may correspond to the surface rupture of the 1912 earthquake under the Gulf of Saros (Karabulut et al. 2006), when its exposed scar across the shelf and its abrupt ending are taken into account. Although L1 appears as a vertical fault on the seismic sections, it actually dips northwards at high angles along the eastern slopes of the inner basin (Fig. 7), suggesting that it may incorporate a slight reverse component.

L2 starts to the immediate north of the western tip of L1, and extends to the SW as a continuous scar. It may be resolved into a number of smaller, curved E-W- and NE-SW-trending segments (Fig. 15). The E-W-trending segments are interpreted to represent oblique extensional faults (Riedel shears), whereas the NE–SW segments would be pure dextral strike–slip faults (P-shear), as revealed by the focal mechanism solutions of the recent earthquakes along this fault (Karabulut et al. 2006). The deformation style (i.e. folding) on both sides of L2 also points to lateral shearing with some vertical movements. Considering the analogue models (Atmaoui et al. 2006), we propose that the E-W-trending segments are synthetic Riedel shears, formed during the early stages of the dextral shear zone development. This was followed by the formation of the NE-SW-trending P-shears, linking the Riedel faults. The curved patterns on L2 resulted from the linkage of R- and P-shears. The dextral movement along the right-stepped P-shears generated dilatation of the E-W-trending Riedel faults during the progressive evolution of the shear zone.

Two alternatives can be considered for the origin of the L3 fault system, which either formed independently of the L2 system as an en-echelon oblique fault system above a NE-SW-trending dextral shear zone (McNeill et al. 2004), or may have formed under the NE–SW extensional stress regime generated by the movement of the left-stepping NE-SW-trending dextral P-shears of L2. In the first alternative, the underlying dextral shear zone would be aligned in a NE–SW direction, but differing in strike by a few degrees from the equally NE-SW-trending L2 segments (060 and 067 respectively). The geometry of L3 suggests that the underlying dextral shear zone is a left-stepping shear zone, since L3 can be resolved into three NE-SW- and two E-W-trending segments. The wider spacing of the en-echelon faults on the NE-SW-trending segments, and the close spacing and merging on the E–W segments suggest that the E–W segments were formed as oblique extensional transfer faults connecting the two neighbouring NE-SW-trending segments.

In the second alternative, the NE-SW-directed extension would be accommodated by the formation of en-echelon fault blocks in the hanging wall of the south-facing Riedel faults on L2. The wider spacing of these oblique NE-SW-trending faults, and the narrow spacing in the WNW–ESE direction would then relate to the left-stepping geometry of the underlying dextral shear zone (Fig. 15). The closely spaced WNW-ESE-trending faults are interpreted as oblique normal faults developed at the releasing zone of the two neighbouring NE-SW-trending dextral shear zone segments.

We favour this second alternative, since most of the Riedel faults of L3 are shallow structures, and the distance between L2 and L3 is very narrow, varying from only 3 to 10 km. The narrowest part of the ID is formed where the E-W-trending segments of both the L2 and L3 fault systems are located on opposite sides of the basin. The width of the basin reaches its maximum where the NE–SW segment of L2 and the E–W segment of L3 form the opposite margins. Thus, at least two rhomboidal basins can be distinguished along the inner depression. We propose that these rhomboidal basins were joined together during the progressive evolution of the dextral shear zone in the course of further dilation of the E-W-trending Riedel faults. The inner depression is therefore considered to be an active, Riedel-type pull-apart basin. The northern limb of the anticline to the immediate north of L3 could be the site of a future Riedel-type rupture in this active system.

Mass-wasting and deposition

Landslides, channel/canyon systems, and deep-sea fans were identified on the multi-beam bathymetric data (Fig. 16). The major landslide on the north-eastern shelf (SLS1) affects a ca. 30-km-long and 6-km-wide area. Several concave scars disrupt the shelf and generate steps in the shelf plain. A more evolved landslide occurs along the northern shelf. The scars of that landslide were eroded by the channel system (C2), but its debris is inferred to have deposited on the smooth slopes to the north of L2. It thus appears that the present northern shelf break retreated
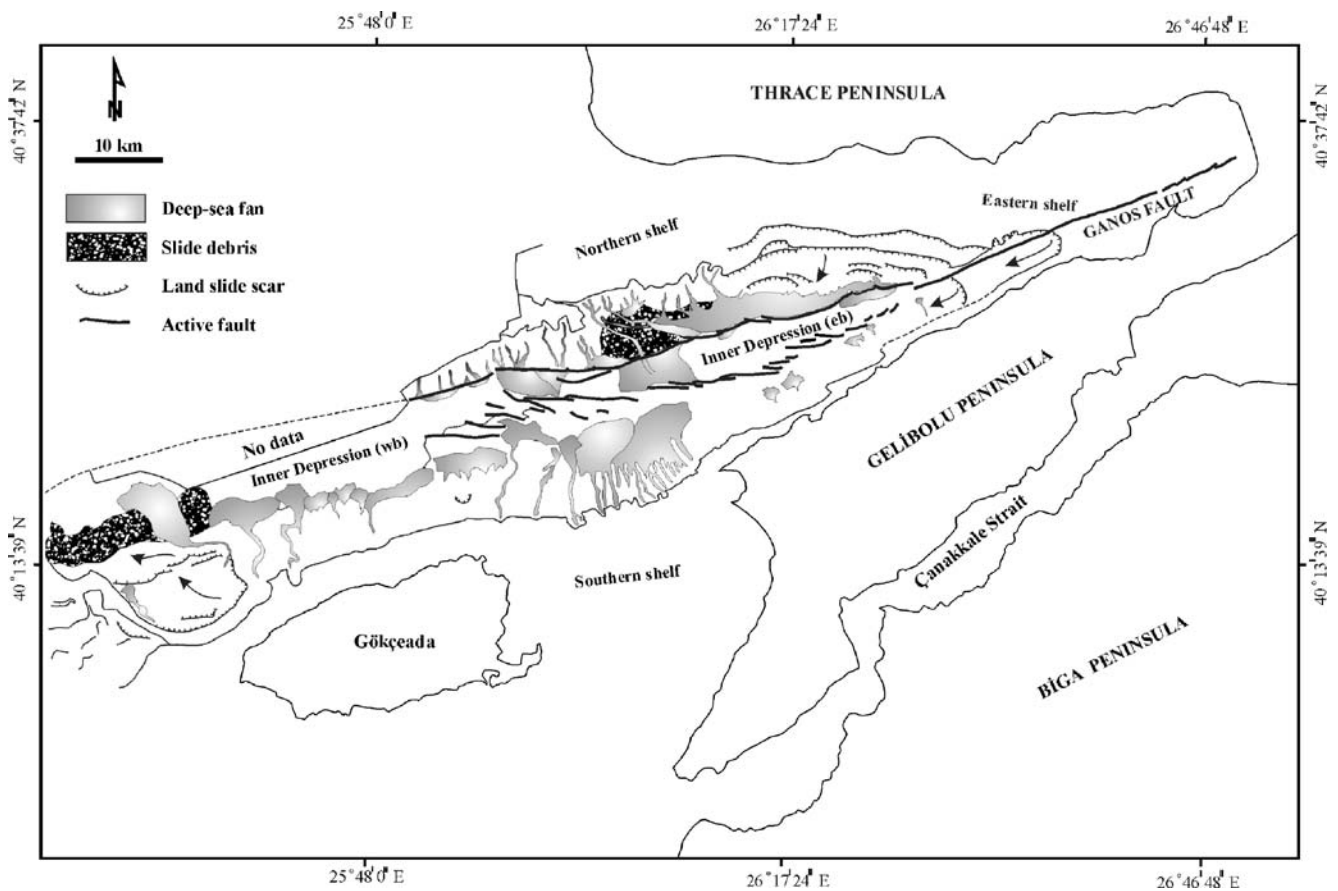
Fig. 16 Map showing the patterns of erosion and deposition in the Gulf of Saros and the NE Aegean Sea. Note the absence of channels and large deep-sea fans to the north of the Gelibolu Peninsula. This is considered to be controlled by the diagenetic state of the rocks exposed in the area. Unconsolidated or relatively weakly consolidated rocks are more easily eroded by mass-wasting processes. *eb* Eastern sub-basin, *wb* western sub-basin

considerably to the north and east. Two landslides are seen on the eastern shelf along the Ganos Fault (L1), where a narrow depression is formed on both sides of the fault. Scars of these landslides indicate that the shelf break retreated by at least 15 km north-eastwards.

Retreat of the southern shelf break is also clearly evident to the NW of Gökçeada. This remarkable landslide (SLS3) affected a 6-km-wide and 15-km-long area, thus transporting a huge volume of debris to the deep western inner depression (Fig. 16). Smaller slides are also present on the western side of this large slide.

As illustrated in Fig. 16, intense channel/canyon incisions have eroded the slopes of the inner basin. Only along the northern slope of the Gelibolu Peninsula are channels rare, all other slopes being subject to mass-wasting, as indicated by the channel systems. We contend that, in addition to landsliding, mass-wasting contributes considerably to the retreat of the shelf breaks around the inner basin. As noted above, the land-derived sediments are mainly trapped on the shelves, as only a few channels cut the shelf break. The majority of the modern channel systems are

therefore thought to have formed by ongoing tectonic activity, responsible for the instabilities of the shelves and slopes of the inner basin.

The channels feed a number of deep-sea fans at the base of slopes. The submarine ridge between the two sub-basins is formed by one of the largest of these fans. It possibly formed by recent deposition of sediments transported from both shelves via canyons C2 and C3. One of the deep-sea fans covers, and hence postdates, the landslides to the NW of Gökçeada. Similarly, a number of channels erode older slide deposits at the base of the northern shelf, and carry the eroded material into the inner depression. The high frequency of deep-sea fans in this region indicates sedimentation to be substantial in the basin.

The modern shelves of the inner basin are dominated by Miocene–Quaternary sediments which unconformably overlie the Eocene volcanic sedimentary successions. The Miocene sedimentary successions (the Enez Basin; Tüysüz et al. 1998) are exposed onland along the western part of the Thrace Peninsula, being dominated by shallow-marine sediments. We consider that these younger deposits are

subject to mass-wasting, thereby controlling the present morphology of the shelves and slopes of the inner basin. The older deposits are more resistant to such mass-wasting processes, due to their advanced diagenetic state. The absence of Miocene–Quaternary sediments along the northern part of the Gelibolu Peninsula thus rather well explains the apparent rarity of landsliding, channel systems, and deep-sea fans along the northern slopes. Once the younger deposits are eroded and reworked into the deep basin, fresh surfaces of older deposits are exposed on the slopes of the basin. Such surfaces are expected to be terraced, with steep slopes and low-angle plains. Thus, modern deep-sea sediments may be deposited directly on older deposits, thereby generating a deep-sea unconformity. Their preservation potential, however, would be low, unless a major change were to occur in the tectonic regime.

Tectonic evolution model

The inner basin was possibly formed as a trans-tensional basin during the Pliocene, as suggested previously by Tüysüz et al. (1998), Kurt et al. (2000) and McNeill et al. (2004). Subsequently, the basin boundary faults gradually became inactive, further deformation being localised and controlled by a new generation of faults in the central part of the basin. These new faults produced the inner depression in the course of the Quaternary.

The evolution of new faults began with the formation of synthetic Riedel shears (L2) dissecting the pre-existing basin fill. The Riedel shears were then linked by P-shears and started to extend in a NE–SW direction. At this stage, en-echelon oblique faults (L3) developed to accommodate the extension, resulting in the generation of small, isolated rhomboidal basins. The basin margins retreated by landsliding and channel erosion, thereby progressively generating a wider basin. The rhomboidal basins were subsequently linked, and subsidence then enabled more sediment to be deposited. Each tectonic pulse triggered mass-wasting in the form of landslides, and through channel systems along the retreating basin margins. Thus, as the shelves eroded, the basin continuously widened and thereby enabled progressively more sediment to be deposited in the subsiding basin. The net result was a wide and deep basin dissected in the central part by a strike–slip fault zone. The basin will probably continue to grow by progressive evolution of the dextral shear zone, and continued mass-wasting of the eastern and northern shelves.

Although there are no borehole data available to assess the sedimentary infill of the inner basin, we infer that the >1,500 m thick succession begins with a thin deposit of shallow-marine sediments, which are overlain by a thick sequence of deep-sea sediments. The latter are expected to be dominated by turbidites and debris flows with occasional "exotic" blocks derived from the slopes. Slump horizons and local unconformities resulting from the ongoing tectonic activity would also be expected to occur. The provenance of the sedimentary fill is mixed, originating initially from the erosion of younger rocks, and subsequently from both younger and older rocks. Land-derived material supplied by rivers can be expected to occur throughout the deposits. We consider, however, that direct sediment input from the adjacent land has played an overall minor role. Although global sea-level changes may have increased the sediment contribution from the land, we propose that, even during glacial periods, the slopes of the basin were the dominant sediment source, as these were unstable due to the ongoing tectonic activity.

Implications of the model for the Marmara Sea

The picture is very similar in the Marmara Sea, which is dissected into three wide rhomboidal basins by a strike–slip fault (the North Anatolian Fault Zone). The shelves and the bordering land areas are dominated by late Miocene, Pliocene and Quaternary continental sediments which unconformably overlie Palaeogene volcanic sedimentary units, similar to the region around the Gulf of Saros. An exception is the Çınarcık Basin, where the surrounding land is composed of Palaeozoic rocks. The southern shelf is broader, whereas the northern shelf is narrow, the slopes being smoother and more gentle in the south and steep in the north.

The strike–slip deformation zone under the Marmara Sea, termed the Main Marmara Fault (İmren et al. 2001; Le Pichon et al. 2001; Şengör et al. 2005) or New Marmara Fault (Gökaşan et al. 2003), forms the eastern submarine continuation of the Ganos Fault (combined L1 and L2 of this study). A tectonic model explaining the active tectonics in the Marmara Sea has previously been suggested on the basis of bathymetric and seismic data (Gökaşan et al. 2001, 2003; İmren et al. 2001; Le Pichon et al. 2001; Kuşçu et al. 2002; Demirbağ et al. 2003; Rangin et al. 2004; Şengör et al. 2005). According to this model, the faults along the basin boundaries of the Marmara Sea are inactive or less active today, and a single continuous dextral fault (NAFZ in the Marmara Sea) cutting the basins and ridges controls the active tectonics. In other words, the model suggests that the fault zone only dissects the basins but did not generate these.

We, on the other hand, suspect that, as in the case of the inner basin in the Saros Gulf and the NE Aegean Sea, the morphology of the deep and wide sedimentary basins in

the Marmara Sea have also been controlled by the activity of this centrally located fault zone, combined with mass-wasting of the conjugate slopes. Large landslides affecting both the northern and southern shelves and slopes of the basins have actually been described previously by Gazioğlu et al. (2002, 2005) and Gökaşan et al. (2003). As in the other areas, the shelf break in the Marmara Sea is also dissected by a number of submarine channel systems.

Unlike the Gulf of Saros, however, the dextral motion of the Main Marmara Fault in the western Marmara Sea is clearly indicated by the right-lateral displacements on the submarine ridges separating the individual basins. The age of this fault is considered to be 200 ka, an estimate based on the lateral offsets of the morphological markers and the geodetic data. However, the displacement rate on the ridges diminishes from west to east, and possibly becomes zero in the north-western corner of the Çınarcık Basin.

Conclusions

The main conclusions of this study are:

1. A SW-NE-trending deep-sea basin, bordered by a wide shelf to the north and east, and a narrow shelf to the south in the Gulf of Saros and the Aegean Sea, has formed by the interaction of tectonics and mass-wasting processes possibly operating since the Pliocene.
2. The North Anatolian Fault propagated into the basin only during the Quaternary. It cuts the eastern shelf and the slope, and abruptly ends at the edge of the inner basin.
3. The present dextral shearing is accommodated by two fault zones bordering the inner depression. The northern boundary fault is a break-through fault, whereas the southern boundary fault is represented by en-echelon, synthetic Riedel faults.
4. The slopes of the inner basin show extensive mass-wasting by landsliding and channel erosion. These processes are interpreted to have been triggered by active faulting, and are considered to be the most effective processes in widening the basins in the study area and in the Marmara Sea.
5. The eroded materials are transported into the deep basins and deposited there in a series of deep-sea fans and slumps. A high sedimentation rate would be responsible for the deposition of over 1,500 m of sediments in the basin.

References

Altunel E, Meghraoui M, Akyüz HS, Dikbas A (2004) Characteristics of the 1912 co-seismic rupture along the North Anatolian Fault Zone (Turkey): implications for the expected Marmara earthquake. Terra Nova 16:198–204

Ambraseys NN, Finkel CF (1987) The Saros–Marmara earthquake of 9 August 1912. Earthquake Eng Struct Dyn 15:189–211

Armijo R, Meyer B, Hubert A, Barka A (1999) Westward propagation of the North Anatolian Fault into the northern Aegean: timing and kinematics. Geology 27:267–270

Armijo R, Meyer B, Navarro S, King G, Barka A (2002) Asymmetric slip partitioning in the Sea of Marmara pull-apart: a clue to propagation process of the North Anatolian Fault. Terra Nova 14:80–86

Armijo R, Pondard N, Meyer B, Uçarkuş G, Mercier de Lépinay B, Malavieille J, Dominguez S, Gustcher M, Schmidt S, Beck C, Çağatay N, Çakır Z, İmren C, Eriş K, Natalin B, Özalaybey S, Tolun L, Lefèvre I, Seeber L, Gasperini L, Rangin C, Emre O, Sarıkavak K (2005) Submarine fault scarps in the Sea of Marmara pull-apart (North Anatolian Fault): implications for seismic hazard in Istanbul. Geochemistry Geophysics Geosystems 6(6):Q06009 doi:10.1029/2004GC000896

Atmaoui N, Kukowski N, Stöckhert B, König D (2006) Initiation and development of pull-apart basins with Riedel shear mechanism: insights from scaled clay experiments. Int J Earth Sci 95:225–238

Barka AA (1992) The North Anatolian fault zone. Ann Tectonics 6 (Special Issue):164–195

Barka AA, Kadinsky-Cade K (1988) Strike–slip fault geometry in Turkey and its influence on earthquake activity. Tectonics 7:663–684

Barka AA, Reilinger R (1997) Active tectonics of the Eastern Mediterranean region: deduced from GPS, neotectonic and seismicity data. Ann Geophys XL:587–610

Bayhan E, Ergin M, Temel A, Keskin (2001) Sedimentology and mineralogy of surficial bottom deposits from the Aegean–Çanakkale–Marmara transition (Eastern Mediterranean): effects of marine and terrestrial factors. Mar Geol 175:297–315

Çağatay N, Görür N, Alpar B, Saatçılar R, Akkök R, Sakınç M, Yüce H, Yaltırak C, Kuşçu (1998) Geological evolution of the Gulf of Saros, NE Aegean Sea. Geo Mar Lett 18:1–9

Coşkun B (2000) North Anatolian Fault–Saros Gulf relationships and their relevance to hydrocarbon exploration, northern Aegean Sea, Turkey. Mar Pet Geol 17:751–772

Cvijic J (1908) Grundlinien der Geographie und Geologie von Mazedonien und Altserbien. Petermans Mitteilungen (Gotha) Ergänzungsheft I(162)

Demirbağ E, Gökaşan E, Oktay FY, Şimşek M, Yüce H (1999) The last sea level changes in the Black Sea: evidence from the seismic data. Mar Geol 157:249–265

Demirbağ E, Rangin C, Le Pichon X, Şengör AMC (2003) Investigation of the tectonics of the Main Marmara Fault by means of deep towed seismic data. Tectonophysics 361:1–19

Elmas A (2003) Late Cenozoic tectonics and stratigraphy of northwestern Anatolia: the effects of the North Anatolian Fault to the region. Int J Earth Sci 92:380–396

Emre O, Erkal T, Tchepalyga A, Kazancı N, Keçer M, Unay E (1998) Neogene–Quaternary evolution of the eastern Marmara Region. Bull Miner Res Explor Inst Turkey 120:223 – 258 (in Turkish)

Erinç S (2000) Geomorphology I, 5th edn. Der Press, Istanbul (in Turkish, modified by Ertek A, Güneysu C)

Erol O, Nuttal CP (1973) Some marine Quaternary deposits in the Dardanelles area. Bull Geogr Invest 5(6):27 – 91 (in Turkish)

Gazioğlu C, Gökaşan E, Algan O, Yücel ZY, Tok B, Doğan E (2002) Morphologic features of the Marmara Sea from multi-beam data. Mar Geol 190(1/2):333–356

Gazioğlu C, Yücel ZY, Doğan E (2005) Morphological features of major submarine landslides of Marmara Sea using multibeam data. J Coast Res 21(4):664–673

Gökaşan E, Demirbağ E, Oktay FY, Ecevitoğlu B, Şimşek M, Yüce H (1997) On the origin of the Bosphorus. Mar Geol 140:183–199

Gökaşan E, Alpar B, Gazioğlu C, Yücel ZY, Tok B, Doğan E, Güneysu C (2001) Active tectonics of the İzmit Gulf (NE Marmara Sea): from high resolution seismic and multi-beam bathymetry data. Mar Geol 175(1/4):271–294

Gökaşan E, Gazioğlu C, Alpar B, Yücel ZY, Ersoy, Gündoğdu O, Yaltırak C, Tok B (2002) Evidence for the NW extension of the North Anatolian Fault Zone in the Marmara Sea; a new approach to the 17 August 1999 Marmara Sea earthquake. Geo Mar Lett 21:183–199

Gökaşan E, Ustaömer T, Gazioğlu C, Yücel ZY, Öztürk K, Tur H, Ecevitoğlu B, Tok B (2003) Morpho-tectonic evolution of the Marmara Sea inferred from multi-beam bathymetric and seismic data. Geo Mar Lett 23(1):19–33

Gökaşan E, Tur H, Ecevitoğlu B, Görüm T, Türker A, Tok B, Çağlak F, Birkan H, Şimşek M (2005) Evidence and implications of massive erosion along the Strait of İstanbul (Bosphorus). Geo Mar Lett 25:324–342

Gökaşan E, Ergin M, Özyalvaç M, Sur Hİ, Tur H, Görüm T, Ustaömer T, Batuk F, Alp H, Birkan H, Türker A, Gezgin E, Özturan M (2007) Factors controlling the present seafloor morphology of the Çanakkale Strait (Dardanelles). Geo Mar Lett (in press). doi:10.1007/s00367-007-0094-y

Görür N, Çağatay MN, Sakınç M, Sümengen M, Şentürk K, Yaltrak C, Tchapalyga A (1997) Origin of the Sea of Marmara as deducted from the Neogene to Quaternary paleogeographic evolution of its frame. Int Geol Rev 39:342–352

Gutzwiller O (1923) Beitrage zur Geologie der Umgebung von Merfete (Mürefte) am Marmara Meer. Ph.D. Thesis, Universität Basel, Basel

İmren C, Le Pichon X, Rangin C, Demirbağ E, Ecevitoğlu B, Görür N (2001) The North Anatolian Fault within the Sea of Marmara: a new evaluation based on multichannel seismic and multi-beam data. Earth Planet Sci Lett 186:143–158

Karabulut H, Roumelioti Z, Benetatos C, Mutlu AK, Özalaybey S, Aktar M, Kiratzi A (2006) A source study of the 6 July 2003 (Mw 5.7) earthquake sequence in the Gulf of Saros (Northern Aegean Sea): seismological evidence for the western continuation of the Ganos fault. Tectonophysics 412:195–216

Ketin İ (1948) Über die tektonisch-mechanischen Folgerungen aus der grossen anatolischen Erdbeben des letzten Dezenniums. Geol Rundsch 36:77–83

Ketin İ (1968) Relations between general tectonic features and the main earthquake regions in Turkey. MTA Bull 71:129–134

Kurt H, Demirbağ E, Kuşçu (2000) Active submarine tectonism and formation of the Gulf of Saros, NE Aegean Sea, inferred from multi-channel seismic reflection data. Mar Geol 165:13–26

Kuşçu Y, Okamura M, Matsuoka H, Awata Y (2002) Active faults in the Gulf of İzmit on the North Anatolian Fault, NW Turkey: a high resolution shallow seismic study. Mar Geol 190(1/2):421–433

Le Pichon X, Şengör AMC, Demirbağ E, Rangin C, İmren C, Armijo R, Görür N, Çağatay N, Mercier de Lepinay B, Meyer B, Saatçiler R, Tok B (2001) The active main Marmara Fault. Earth Planet Sci Lett 192:595–616

McNeill LC, Mille A, Minshull TA, Bull JM, Kenyon NH, Ivanov M (2004) Extension of the North Anatolian Fault into the North Aegean Trough: evidence for transtension, strain partitioning, and analogues for Sea of Marmara basin models. Tectonics 23: TC2016 doi:10.1029/2002TC001490

Okay A, Demirbağ E, Kurt H, Okay N, Kuşçu (1999) An active, deep marine strike–slip basin along the North Anatolian fault in Turkey. Tectonics 18(1):129–147

Okay AI, Tüysüz O, Kaya (2004) From transpression to transtension: changes in morphology and structure around a bend on the North Anatolian Fault in the Marmara region. Tectonophysics 391: 259–282

Pamir HN (1938) On the problem about the formation of the Strait of İstanbul. Bull Miner Res Explor Inst Turkey 3/4:61 – 69 (in Turkish)

Pfannenstiel M (1944) Diluviale Geologie des Mittelmeergebietes, die diluvialen Entwicklungstadien und die Urgeschichte von Dardanellen, Marmara Meer und Bosphorus. Geol Rundsch 34:334–342

Rangin C, Le Pichon X, Demirbağ E, İmren C (2004) Strain localization in the Sea of Marmara: propagation of the North Anatolian Fault in a now inactive pull-apart. Tectonics 23(2): TC2014 doi:10.1029/2002TC001437

Saatçılar R, Ergintav S, Demirbağ E, İnan S (1999) Character of active faulting in the North Aegean Sea. Mar Geol 160:339–353

Saner S (1985) Sedimentary sequences and tectonic setting of Saros Gulf region NE Aegean Sea, Turkey. Bull Geol Soc Turkey 28:1 – 10 (in Turkish)

Şaroğlu F, Emre Ö, Kuşçu (1992) Active fault map of Turkey. Scale 1: 2.000.000. General Directorate Mineral Research and Exploration, Ankara (in Turkish)

Seeber L, Emre O, Cormier MH, Sorlien CC, McHugh CMG, Polonia A, Ozer N, Cagatay N (2004) Uplift and subsidence from oblique slip: the Ganos–Marmara bend of the North Anatolian Transform, Western Turkey. Tectonophysics 391:239–258

Şengör AMC (1979) The North Anatolian Transform Fault; its age offset and tectonic significance. J Geol Soc Lond 136:269–282

Şengör AMC, Görür N, Şaroğlu F (1985) Strike–slip faulting and related basin formation in zones of tectonic escape: Turkey as a case study. Soc Econ Paleontol Mineral Spec Publ 37: 228–264

Şengör AMC, Tüysüz O, İmren C, Sakınç M, Eyidoğan H, Görür N, Le Pichon X, Rangin C (2005) The North Anatolian Fault: a new look. Annu Rev Earth Planet Sci 33:1–75

Siyako M, Burkan KA, Okay A (1989) Tertiary geology and hydrocarbon potential of the Biga and Gelibolu peninsulas. Bull Turkish Assoc Petrol Geol 1(3):183 – 200 (in Turkish)

Sümengen M, Terlemez I, Şentürk K, Karaköse C, Erkan E, Ünay E, Gürbüz M, Atalay Z (1987) Stratigraphy, sedimentology, and tectonics of the Tertiary sequences in Gelibolu Peninsula and southwestern Thrace. Bulletin of the Mineral Research and Exploration Institute of Turkey Technical Report 8128 (in Turkish)

Taymaz T, Jackson J, McKenzie D (1991) Active tectonics of the north and central Aegean Sea. Geophys J Int 106:433–490

Tüysüz O, Barka AA Yiğitbaş E (1998) Geology of the Saros Graben: its implications on the evolution of the North Anatolian Fault in the Ganos–Saros Region, NW Turkey. Tectonophysics 293: 105–126

Yaltırak C, Alpar B (2002) Kinematics and evolution of the northern branch of the North Anatolian Fault (Ganos Fault) between the

Sea of Marmara and the Gulf of Saros. Mar Geol 190(1/2): 351–366

Yaltırak C, Alpar B, Yüce H (1998) Tectonic elements controlling the evolution of the Gulf of Saros (northeastern Aegean Sea, Turkey). Tectonophysics 300:227–248

Yaltırak C, Alpar B, Sakınç M, Yüce H (2000) Origin of the Strait of Çanakkale (Dardanelles): regional tectonics and the Mediterranean–Marmara incursion. Mar Geol 164:139–159

Yaltırak C, Sakınç M, Aksu AE, Hiscott RN, Galleb B, Ulgen UB (2002) Late Pleistocene uplift history along the southwestern Marmara Sea determined from raised coastal deposits and global sea-level variations. Mar Geol 190(1/2):283–305

Yiğitbaş E, Elmas A, Sefunc A, Özer N (2004) Major neotectonic features of eastern Marmara Region, Turkey: development of the Adapazarı–Karasu corridor and its tectonic significance. Geol J 39:179–198

Yılmaz Y (2007) Morphotectonic evolution of the Southern Black Sea Region and the Bosphorus Channel. In: Yanko-Hombach V (ed) The Black Sea Flood question: changes in the coastline, climate, and human settlement. NATO Science Series IV, Earth and Environmental Sciences (in press)

Zattin M, Okay AI, Cavazza W (2005) Fission-track evidence for late Oligocene and mid-Miocene activity along the North Anatolian Fault in south-western Thrace. Terra Nova 17:95–101